ORGANISMAL BIOLOGY

A brain microbiome in salmonids at homeostasis

Amir Mani[1], Cory Henn[1], Claire Couch[2], Sonal Patel[3], Thora Lieke[4], Justin T.H. Chan[5,6], Tomas Korytar[4,6], Irene Salinas[1]*

Ectotherms have peculiar relationships with microorganisms. For instance, bacteria are recovered from the blood and internal organs of healthy teleosts. However, the presence of microbial communities in the healthy teleost brain has not been proposed. Here, we report a living bacterial community in the brain of healthy salmonids with bacterial loads comparable to those of the spleen and 1000-fold lower than in the gut. Brain bacterial communities share >50% of their diversity with gut and blood bacterial communities. Using culturomics, we obtained 54 bacterial isolates from the brains of healthy trout. Comparative genomics suggests that brain bacteria may have adaptations for niche colonization and polyamine biosynthesis. In a natural system, Chinook salmon brain microbiomes shift from juveniles to reproductively mature adults. Our study redefines the physiological relationships between the brain and bacteria in teleosts. This symbiosis may endow salmonids with a direct mechanism to sense and respond to environmental microbes.

INTRODUCTION

Brain-microbiota communication at homeostasis is governed by microbial-derived chemical mediators and metabolites that directly or indirectly signal to the brain (*1*–*3*). During homeostasis, however, viable microorganisms may leak from the gut forming complex microbial communities in gut-distal tissues including lymph nodes and liver, according to mammalian studies (*4*–*6*). Still, the presence of microbial communities in the vertebrate brain remains highly controversial and only associated with disease states. Evidence for the presence of microorganisms in the diseased human brain is accumulating (*7*–*10*), but whether brain microbiomes occur at homeostasis remains an unanswered question.

Teleosts appear to be especially permissive to the presence of bacteria in their internal organs during homeostasis. For instance, culturable bacteria could be recovered from the blood and kidneys of healthy salmonids (*11*); the biological and functional significance of this observation is still unexplored. More recently, the microbial communities from the spleen of healthy and diseased tilapia were sequenced (*12*), and blood microbiomes have been proposed as a health biomarker in halibut (*13*). This peculiar relationship between teleosts and systemic bacteria is further illustrated by an overall lack of an endotoxic shock response to lipopolysaccharide (LPS) injection, a 60-year-old observation that further underscores that teleost internal organs coexist with bacteria (*14*, *15*). Together, these findings motivated us to hypothesize that bacteria and teleosts form a symbiosis in the brain under physiological states.

Here, we show that in salmonids, microbiota directly colonize brain tissues and display some signatures of adaptation to this niche. While the exact physiological implications of bacterial presence in the teleost brain are yet to be fully understood, our findings suggest that microbiota regulates the teleost brain not only via the canonical gut-brain axis but also by direct colonization of this organ. This work opens up research avenues in understanding microbiota-driven neuromodulation in natural systems as well as in farmed fish.

RESULTS

Viable bacteria are found in all brain regions of laboratory-reared rainbow trout

The presence of bacteria in the healthy brain is a matter of debate (*16*–*20*). Under physiological conditions, culturable bacteria can be recovered from the blood and other internal organs of teleosts (*11*–*13*). Thus, we sought to investigate whether the teleost brain is also colonized by bacteria at the steady state. We first quantified bacterial levels in four brain regions [olfactory bulb (OB), telencephalon (Tel), optic tectum (OT), and cerebellum (Cer)] as well as the gut, spleen, and blood of juvenile, laboratory-reared rainbow trout. Animals were perfused before sampling to remove any blood contamination from the brain. The efficacy of the perfusion was verified by quantifying hemoglobin levels before and after the perfusion. This confirmed a perfusion efficiency of 99.1 to 99.4% depending on the tissue (fig. S2, F to H). Bacterial loads in the Tel, OT, and Cer were comparable to those found in the spleen and three orders of magnitude lower than in the gut. In the OB, bacterial loads were significantly lower than in the rest of the brain regions examined. In the blood, bacterial levels were the lowest, with 4.6×10^3 16*S* copies/μg of tissue or blood DNA compared to 1.9×10^4 in the spleen (Fig. 1A). Using RNA as a template, estimated bacterial loads were comparable to those using DNA as a template (Fig. 1B). The presence of bacterial RNA in the brain suggests that bacteria are viable. To confirm this, we applied culturomics approaches to grow trout gut, blood, spleen, and brain bacterial isolates in different growth media: Luria-Bertani (LB), nutrient broth (NB), tryptic soy broth (TSB), MacConkey and Frey Mycoplasma broth base; under aerobic and anaerobic conditions, different temperatures (16°C, room temperature, and 30°C) and lysis methods (see the Supplementary Materials). We also obtained cerebrospinal fluid (CSF) from the same animals and plated it under the same conditions. Using an NP-40 detergent extraction protocol under either aerobic or anaerobic conditions (Fig. 1C), we recovered 1.9×10^3 to 2×10^3 colony-forming units (CFUs)/g of

[1]Center for Evolutionary and Theoretical Immunology, Department of Biology, University of New Mexico, Albuquerque, NM 87108, USA. [2]Department of Fisheries, Wildlife, and Conservation Sciences, Oregon State University, Corvallis, OR 97331, USA. [3]Norwegian Veterinary Institute, Thormøhlens Gate 53C, 5006 Bergen, Norway. [4]Faculty of Fisheries and Protection of Waters, South Bohemian Research Center of Aquaculture and Biodiversity of Hydrocenoses, Institute of Aquaculture and Protection of Waters, University of South Bohemia, České Budějovice, Czech Republic. [5]Fish Health Division, University of Veterinary Medicine, Vienna, Austria. [6]Institute of Parasitology, Biology Centre of the Czech Academy of Sciences, České Budějovice, Czech Republic.
*Corresponding author. Email: isalinas@unm.edu

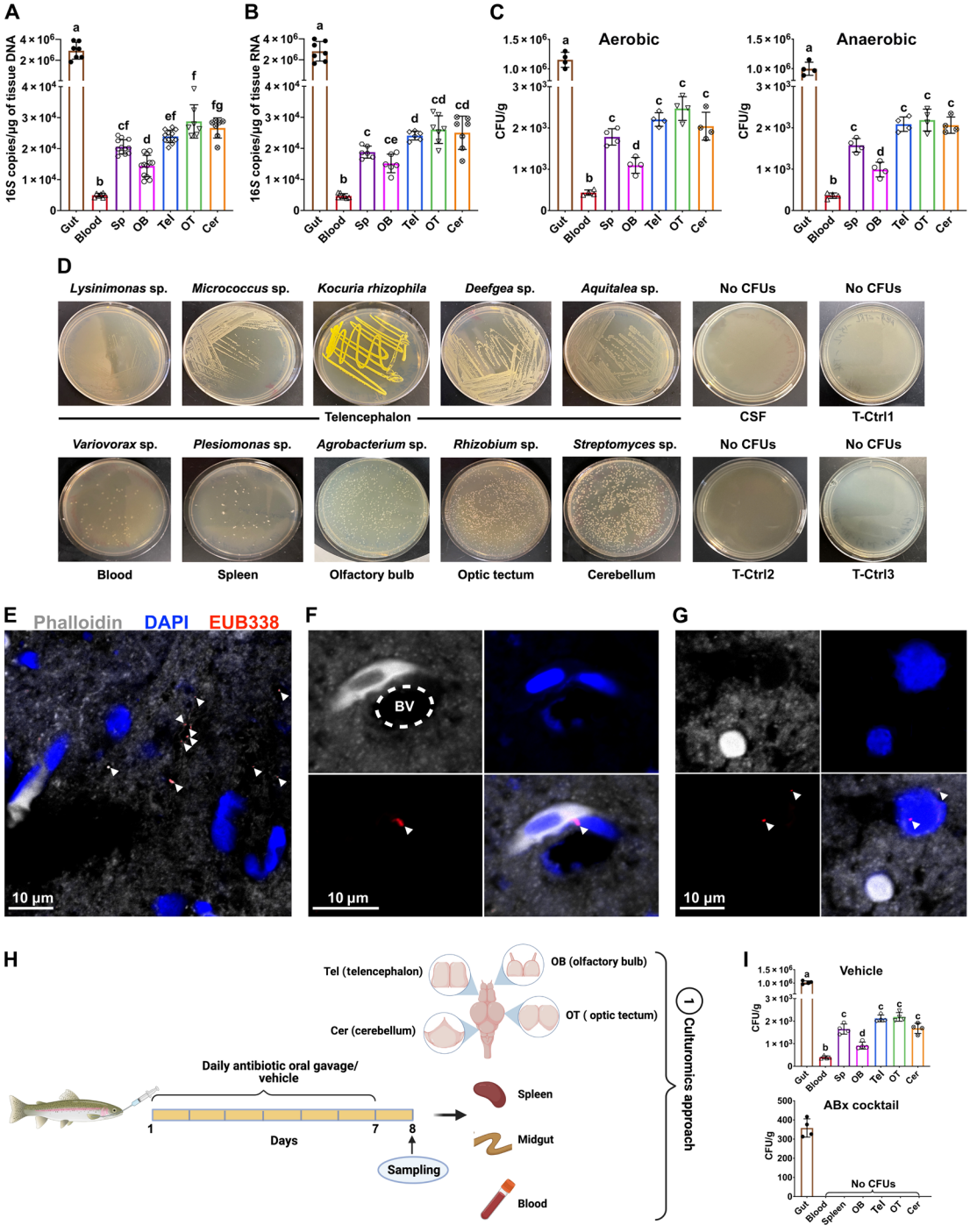

Fig. 1. The healthy rainbow trout brain has living bacteria at homeostasis. (**A** and **B**) Quantification of 16*S* rDNA copies in gut, blood, spleen, and four brain regions (OB, Tel, OT, and Cer) of laboratory rainbow trout using DNA (A) or RNA (B) as a template ($n = 7$). (**C**) Colony-forming units (CFUs) per gram of tissue obtained using the NP-40 lysis method under aerobic and anaerobic conditions at room temperature in tryptic soy agar (TSA) ($n = 4$). Different letters denote statistically significant differences ($P < 0.05$) by Welch's ANOVA test. (**D**) Representative examples of different bacterial isolates from control rainbow trout generated via culturomics efforts. Note that plates seeded with cerebrospinal fluid (CSF) and plates used as technical controls (T-Ctrl1–3) showed no CFUs. (**E** to **G**) Fluorescence in situ hybridization of control trout Tel cryosections using a universal EUB338 oligoprobe (red). In (E), bacteria appear to be located in the brain parenchyma; in (F), bacteria appear to be crossing the blood-brain barrier; and in (G), bacteria appear in close association with cell nuclei, suggesting an intracellular localization. Nuclei were stained with 4′,6-diamidino-2-phenylindole (DAPI; blue) and F-actin was stained with phalloidin (white). Arrowheads indicate bacterial cells. BV, blood vessel. (**H**) Experimental design overview for the antibiotic cocktail oral gavage experiment. (**I**) Number of CFUs recovered from different tissues 1 day after the end of the antibiotic gavage (ABx) trial ($n = 4$). Tissue samples were subjected to NP-40 lysis and CFUs per gram of tissue were counted under aerobic and anaerobic conditions at room temperature for both the vehicle group (top) and the ABx group (bottom). No CFUs were recovered under anaerobic conditions in the antibiotic-gavaged animals. CFU counts correspond to growth on TSA media at room temperature.

tissue in the Tel, OT, and Cer, whereas we obtained 8.9×10^2 CFUs/g in the OB. Similar results were obtained when using the mechanical lysis method under aerobic and anaerobic conditions (fig. S1, A and B). A full summary of our culturomics efforts is shown in table S1. No bacteria were recovered from CSF samples using culturomics (Fig. 1D), and no polymerase chain reaction (PCR) product could be amplified using 16*S* rDNA specific primers (fig. S2J). Similarly, we recovered no colonies in the plates seeded with lysis buffer only as a negative control (Fig. 1D). Bacterial isolates were identified by 16*S* amplicon PCR using Sanger sequencing. A total of 54 isolates were recovered from different trout brain regions and different animals (table S1) and 120 isolates were obtained from all tissues sampled. Representative examples of bacterial cultures from the healthy trout brain and other tissues are shown in Fig. 1D. A few colonies were recovered from the laboratory environment swabs (fig. S2, A and D) but their taxonomic identity did not match any of the fish-derived isolates (fig. S2, B and C). Together, all our rigorous controls confirmed that the recovered culturable bacteria from the trout brain were not environmental contaminants.

We confirmed that bacteria are localized in the brain parenchyma from all regions examined using fluorescence in situ hybridization with universal eubacterial probes (fig. S1, F to K). To further resolve the localization of these bacteria, we costained sections with phalloidin–Alexa Fluor 555. We found bacteria in the brain parenchyma that did not seem to be inside any cells (Fig. 1E). In addition, some bacteria were found closely associated with cell nuclei and appeared to be intracellular (Fig. 1G). The identity of the cells was not further resolved. Our attempts to further segment cells by labeling cell membranes on fixed and permeabilized trout brain cryosections failed. Thus, future efforts to elucidate the exact localization of bacteria will be required. Phalloidin staining allowed us to visualize the blood-brain barrier (Fig. 1F), and we were able to observe bacteria that appeared to be crossing the blood-brain barrier, indicating that the blood is likely a source of brain bacteria in trout (Fig. 1F). To corroborate the findings from our microscopy observations using eubacterial probes and given that *Mycoplasma* sp. dominates the gut microbiome of salmonids (*21*–*26*), we designed a Mycoplasma-specific oligonucleotide probe and stained brains from laboratory rainbow trout specimens. *Mycoplasma* sp. could be detected in the brain parenchyma, sometimes closely associated with cell nuclei, suggesting an intracellular localization (fig. S1, C and D).

To support these findings, we performed an in vivo oral gavage experiment using an antibiotic cocktail for 7 days (Fig. 1H) and sampled the gut, spleen, blood, and different brain regions for culturomics experiments. Antibiotic treatment eliminated all CFUs from the blood, spleen, and gut, whereas a few bacterial colonies, all with similar morphology, could still be recovered from the gut (Fig. 1I and fig. S1E). These experiments further substantiate that trout brain bacteria are not the result of experimental contaminations or artifacts. Combined, our results indicate that the brain of healthy rainbow trout, similar to the blood and spleen, contains viable bacteria at homeostasis.

Trout brain bacterial communities are only partly sourced by the gut and blood microbiomes

Previous studies in mammals suggest that internal microbiomes originate from the leakage of gut bacteria into gut-distant organs (*4*–*6*). While internal microbiomes in teleosts have been described, their origins are unknown. To resolve this question, we profiled the bacterial communities in all seven tissues sampled in Fig. 1. At the phylum level, the gut bacterial community was largely dominated by Firmicutes, as previously reported in rainbow trout (Fig. 2, A and B) (*27*–*29*). In the blood, Proteobacteria and Actinobacteria dominated the community, whereas in the spleen, Firmicutes and Proteobacteria were the two dominant phyla. In the four brain regions sampled, Proteobacteria and Actinobacteria were the dominant phyla (63.51 to 81.34%) followed by Firmicutes which accounted for 3 to 15% of the bacterial community (Fig. 2A). At the family level, the gut bacterial community is predominantly composed of Mycoplasmataceae (76.2%) and Chitinobacteriaceae (17.1%) (Fig. 2B). However, Chitinobacteriaceae accounts for only 1 and 1.8% of the total bacterial communities in the blood and spleen, respectively (Fig. 2B). In contrast, this family is consistently present in all brain samples, comprising between 13.91 and 17.57%, a similar abundance to that found in the gut (Fig. 2B). Burkholderiaceae and Propionibacteriaceae, frequently reported in salmonids gut and blood (*30*–*34*), were only detected in the blood (25.44 and 28.07%, respectively) (Fig. 2B). Propionibacteriaceae emerged as the most frequently detected bacterial family in the rainbow trout brain, with relative abundances of 28.5% in the OB, 19.6% in the Tel, 41.7% in the OT, and 28.3% in the Cer (Fig. 2B). Mycoplasmataceae also showed variable frequencies across the brain regions, with higher abundances in the Tel and OT (14.9 and 11.3%, respectively) compared to the OB and Cer (5.6 and 3%, respectively) (Fig. 2B). In addition, Burkholderiaceae accounted for 12.7% of reads in the Cer, while only 4.9% in the OB (Fig. 2B). Enterobacteriaceae accounted for 16.7 and 22.2% of the overall diversity in the blood and spleen, respectively, but were at low relative abundance (<3%) in the rainbow trout brain. Principal coordinates analysis (PCoA) showed tight clustering of the microbial communities from all four regions of the brain and all individuals (Fig. 2C). Water samples clustered apart from all the trout tissue samples sequenced (Fig. 2C and fig. S3). Alpha diversity was lowest in the gut, as previously described in rainbow trout (*27*–*29*) followed by the blood. The highest alpha diversity was found in the OB and Tel (Fig. 2D and table S2). We next compared the beta diversity of each microbial community to that of the gut and found significant differences in the weighted UniFrac distances among tissues (Fig. 2E). The greatest distance was observed between the gut and the blood followed by the distance between the gut and each brain region sampled (Fig. 2E). We did not find significant differences when different brain regions were compared to each other. These results suggest that leakage of bacteria from the gut is not the only source of the blood-circulating microbiome or the brain microbiome in rainbow trout.

To resolve the source of the brain bacterial community, we performed SourceTracker2 analyses using water, gut, or blood as potential sources. Depending on the region, gut sources accounted for 19.7 to 38.7% of all reads, whereas the blood accounted for 20.6 to 50.2% of all reads in the brain (Fig. 2, F and G). Less than 4% of the brain reads originated from the water. Unknown sources not included in our analyses accounted for 20.4 to 46% of all reads in the brain, depending on the region. A breakdown of the diversity present in the unknown sources for all our SourceTracker2 analyses is shown in file S3. Next, we performed statistical analysis to determine whether different brain regions have significantly greater contributions of bacteria of one origin or another. We found that in the Cer, water contributed to the overall diversity at significantly higher proportions than in other brain regions ($P = 0.0137$), whereas the greatest unknown sources were found in the OB (table S3, $P = 0.0066$).

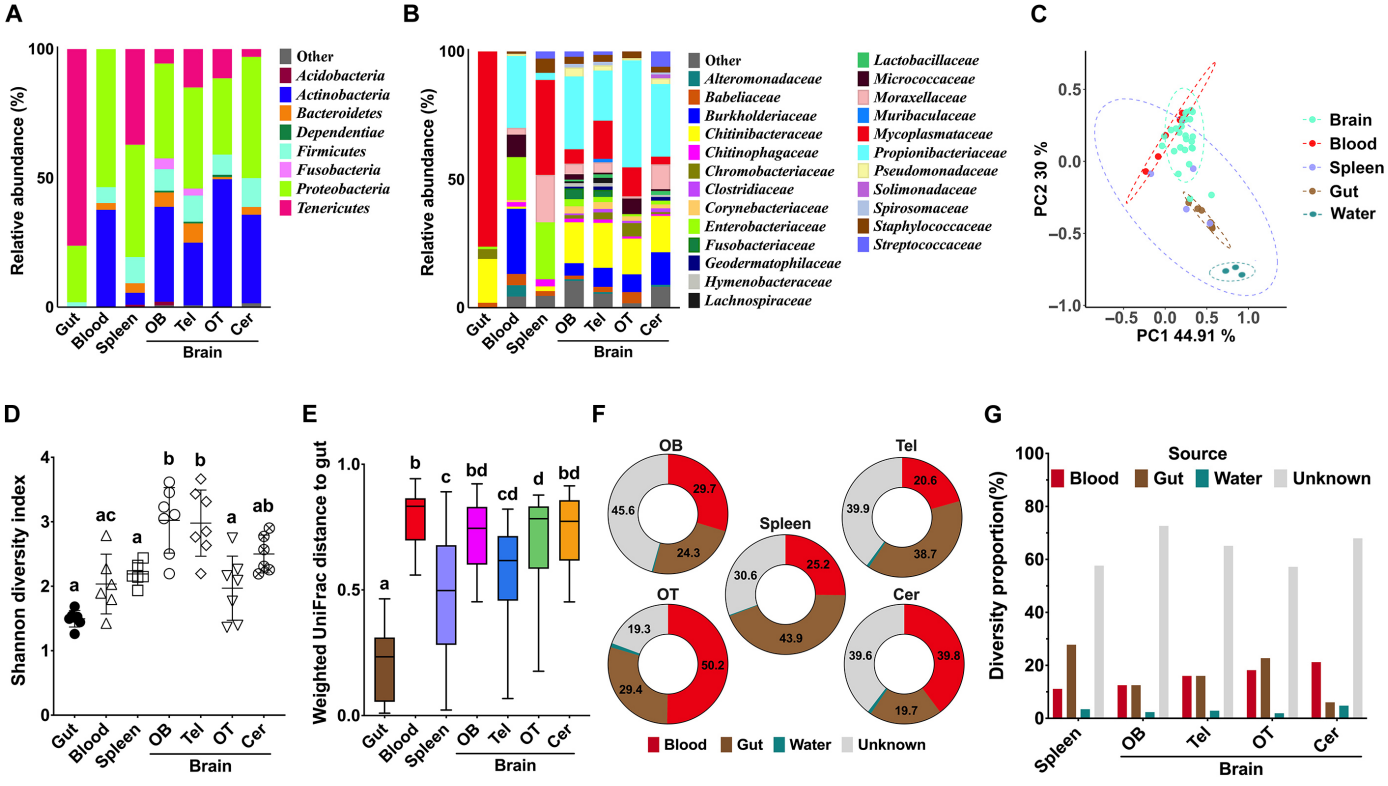

Fig. 2. Diversity, composition, and sources of the brain bacterial community in rainbow trout. (**A** and **B**) Relative abundance of bacterial phyla (A) and families (B) across the gut, blood, spleen, and four brain regions: OB, Tel, OT, and Cer sampled in this study ($n = 7$). (**C**) Principal coordinates analysis (PCoA) of the rainbow trout gut, blood, spleen, and brain microbial communities as well as the water microbial community. Ellipses represent a 95% confidence interval. (**D**) Mean Shannon diversity index of rainbow trout gut, blood, spleen, and brain microbial communities. Different letters indicate statistically significant differences ($P < 0.05$) by the Kruskal-Wallis test. (**E**) Weighted UniFrac distance for rainbow trout gut, blood, and spleen and the four different brain regions sampled ($n = 7$). Different letters indicate statistically significant differences ($P < 0.05$) by Tukey's post hoc test. (**F**) Predicted relative percentage of bacterial reads in the spleen, OB, Tel, OT, and Cer (sinks) originating from the blood, gut, water, or unknown sources using SourceTracker2 analysis. (**G**) Predicted proportion of the overall spleen and brain (OB, TL, OT, and Cer) (sinks) microbial diversity that originates from the blood, gut, water, or unknown sources.

Next, we considered the gut, blood, and spleen as potential sources and the different brain regions as a sink. In this case, SourceTracker2 predicted that the gut (up to 38.7% in the Tel) and blood (up to 50.2% in the OT) still appeared as the predominant sources of the brain microbial community (Fig. 2F and fig. S8), with a minor fraction ranging from 5.6 to 14%, traced back to the spleen (fig. S8A). The contribution from water remained largely unaffected (Fig. 2F and fig. S8). Our taxonomic analysis of the "unknown source" category identified that these were mostly members of the families Propionibacteriaceae (15.1% in OB, 13% in Tel, 9.8% in OT, and 8.1% in Cer), Chitinibacteraceae (7.5% in OB, 9% in Tel, 2.3% in OT, and 4.4% in Cer), and Pseudomonadaceae (6.3% in OB, 4.7% in OT, and 2.5% in Cer) (file S3). Propionibacteriaceae are abundant members of the trout skin microbiome in our laboratory (*26*), suggesting that some mucosal surfaces not sampled in our study, such as the skin, could explain some of the unknown source category (file S3). In the spleen, "unknown" was mainly comprised of Moraxellaceae (31.8%), Staphylococcaceae (21.7%), and Chitinophagaceae 10.8% (file S3), again suggesting potential contributions from the skin as well as the olfactory organ, especially for the Staphylococcaceae (*26*). Our data revealed that the gut and blood constitute the main contributors to the brain microbial community, with a small share associated with the spleen (fig. S8, A to E).

In terms of source for the overall brain microbial diversity, SourceTracker2 predicted that the gut and blood microbiomes combined could only explain up to 40% of the bacterial diversity found in the brain, depending on the region (Fig. 2G). Water only contributed to 1.9 to 4.9% of the overall brain amplicon sequence variant (ASV) diversity. In each of the four brain regions analyzed, we did not detect any differences in the proportion of microbial diversity originating from the gut and blood except for the Cer where the blood's contribution to microbial diversity was significantly higher (21.2%) compared to the gut (6.1%; $P = 0.00152$; table S3). Combined, our results indicate that the brain bacterial community of healthy rainbow trout is partially sourced from the gut and the blood, with additional unsampled sources or a brain core microbiome accounting for the remaining diversity of the community. These results are supported by culturomics results shown in table S1, with some bacterial species found in the brain but not recovered from the gut, blood, or spleen.

Feeding but not daytime affects gut and blood bacterial loads but not brain bacterial loads

Previous work in mammals demonstrated circadian oscillation in gut microbiota shaped by feeding-entrained rhythmicity of daily gut immunoglobulin A (IgA) secretion (*35*). In teleosts, skin microbiomes display rhythmicity too (*36*). We performed a time series

experiment for 30 hours. Animals were fed at 9:00 a.m. on the first morning of the experiment (fig. S4). We monitored blood glucose levels and observed a peak in blood glucose 17 hours after feeding (fig. S4). This slow glucose kinetics are in line with previous reports in trout (*37*–*39*). Bacteria loads associated with the midgut decreased after 12 hours (fig. S4), the exact same time when food reached the midgut. Decreased gut bacterial loads were paralleled by increased blood bacterial loads at the same time (fig. S4), suggesting perhaps a leakage event from the gut to the blood upon ingesta arrival, a hypothesis that requires further investigation. In turn, bacterial loads in two regions of the brain examined remained unaltered (fig. S4). These data suggest that feeding and daytime do not affect brain bacterial loads. However, taxa-specific changes were not quantified and therefore we cannot rule out that oscillatory changes in brain microbiome composition occur upon feeding or with the circadian cycle.

Whole-genome sequencing of brain-resident bacterial isolates identifies potential strategies for brain colonization and niche adaptation

In mammals, pathobionts leaking from the gut into internal compartments undergo within-host evolution to adapt to specific niches (*40*). Given the highly different metabolic environments that bacteria are exposed to in the gut, blood, and brain, we explored potential signatures of niche adaptation in isolates of the same bacterial species from different body locations from two different laboratory rainbow trout. We took advantage of our biorepository of bacterial isolates from rainbow trout gut, blood, and brain to perform comparative genomics. We sequenced whole genomes of *Plesiomonas* sp. and *Agrobacterium* sp., both well-known members of the teleost gut microbiome (*41*–*47*), although *Plesiomonas* sp. has also been reported in diseased teleosts (*48*–*50*). We sequenced *Plesiomonas* sp. isolates from the gut ($n = 5$), blood ($n = 5$), and brain ($n = 6$) and *Agrobacterium* sp. isolates from the gut ($n = 5$), blood ($n = 5$), and brain ($n = 4$) (tables S4 and S5). All isolates came from two individual fish. We first generated a pan-genome for each bacterial species (Fig. 3A and fig. S6A). Trout *Plesiomonas* sp. genomes showed astounding diversity depending on their niche. While some isolates (named "long genome" hereafter) contained 4193 genes and 5,020,997 base pairs (bp), others (named "short genome" hereafter) only contained 2615 genes and 3,121,923 bp (tables S4 and S5). In the gut and the blood, both short- and long-genome Plesiomonas isolates were found, whereas in the brain, only long-genome Plesiomonas was present (Fig. 3B and tables S4 and S5), suggesting that the coexistence of long- and short-genome Plesiomonas does not occur in the brain niche. Comparative genomic analysis highlighted that while both isolates have 44% of annotated genes categorized as enzymes, a higher percentage of transporter proteins (12% compared to 6%) and transcriptional regulators (4% compared to 2%) were observed in the long-genome *Plesiomonas* sp. (Fig. 3C). This differential gene distribution may confer a selective advantage relevant to the unique environmental pressures within the brain niche. Phylogenetic tree analyses of Plesiomonas genomes from our study and other publicly available revealed that our isolates are more closely related to other fish *Plesiomonas* sp. isolates and that all long-genome isolates cluster separately from gut and blood short-genome isolates (Fig. 3D). These results are in agreement with core genome and pan-genome analyses which identified extensive genetic diversity and the presence of large and variable gene repertoires in *Plesiomonas shigelloides* (*51*).

Polyamines are produced by both eukaryotes and prokaryotes, including the gut microbiota (*52*, *53*). In bacteria, polyamines have essential and nonessential roles in growth, biofilm formation, and virulence (*53*). Whereas putrescine and spermidine biosynthesis is widespread among bacteria, spermine production is restricted to some taxa, although it can be taken from the environment (*54*–*56*). Microbiota-derived polyamines such as putrescine contribute to host intestinal homeostasis (*52*). Kyoto Encyclopedia of Genes and Genomes (KEGG) pathway reconstruction of our Plesiomonas genomes identified 39 modules that were significantly enriched in long-genome Plesiomonas versus short-genome Plesiomonas mostly related to metabolism (Fig. 3E, fig. S5A, and table S6). We focused on the stark differences detected in polyamine metabolism modules. All isolates, regardless of the tissue of origin, ubiquitously encode for *odc* (*speC)* (Fig. 3, F and G). However, arginase (*arg*), which catalyzes L-ornithine formation from L-arginine), and *speE* (spermidine synthase, essential for the production of spermidine from putrescine) are only found in long-genome isolates (Fig. 3, F and G). Nucleotide alignments of those isolates expressing *arg* and *speE* revealed no sequence diversity among brain isolates (file S2). In support, we measured polyamine production (putrescine, spermidine, and spermine) by each *Plesiomonas* sp. isolate from 10 isolates using enzyme-linked immunosorbent assay (ELISA). To rule out uptake from the culture medium, we measured polyamine levels in the culture medium alone and found them below detection levels in our assay. Our data show that, as predicted from their genomes, all isolates produced similar levels of putrescine and spermine (in low amounts) regardless of the size of their genome and tissue origin, but spermidine production (which is catalyzed by *speE*) was 10- to 15-fold higher in *Plesiomonas* sp. isolates with long genomes compared to those with short genomes regardless of their tissue origin (Fig. 3H). These results suggest that trout microbiota de novo synthesize polyamines in vitro and that acquisition of genes involved in polyamine biosynthesis may mediate adaptation to the brain niche, a hypothesis that will require further experimental testing in vivo.

We also identified differences in type 3 and type 6 secretion systems copy numbers, which were more abundant in the long-genome *Plesiomonas* sp. isolates (fig. S5B). Furthermore, the capability to produce capsular components via the presence of BDMLBD_07845, GIKMPH_18825, and JOMBDB_16565 genes (Prodigal) (*57*) and to traverse the blood-brain barrier by encoding for endothelial adhesion molecules such as beA, IbeB, IbeC, and IcsA was restricted to the long-genome *Plesiomonas* sp. (fig. S5A). Collectively, our data indicate that adaptations of bacteria to the brain niche consist of (i) unique abilities to penetrate the blood-brain barrier, (ii) ability to outcompete other bacteria and/or evade the immune system, and (iii) production of spermidine which, in turn, could regulate cognitive function, neuroprotection, brain immunity, and blood-barrier permeability (*58*–*62*). These data underscore the genomic plasticity of *Plesiomonas* sp. within a host and the ability of this species to adapt to diverse niches with specific nutritional requirements.

In the case of *Agrobacterium* sp. genomes, genome size and number of genes/genome were not different among isolates from different tissues (6,016,588 bp and 5677 genes; fig. S6, A to C, and tables S4 and S5). Phylogenetic tree analyses indicate that trout-derived Agrobacterium isolates form a distinct clade, diverging as an outgroup relative to the human clinical– and plant-based isolates (fig. S6B). Multiple amino acid sequence variation was identified in brain-resident *Agrobacterium* sp. exopolysaccharide biosynthesis gene

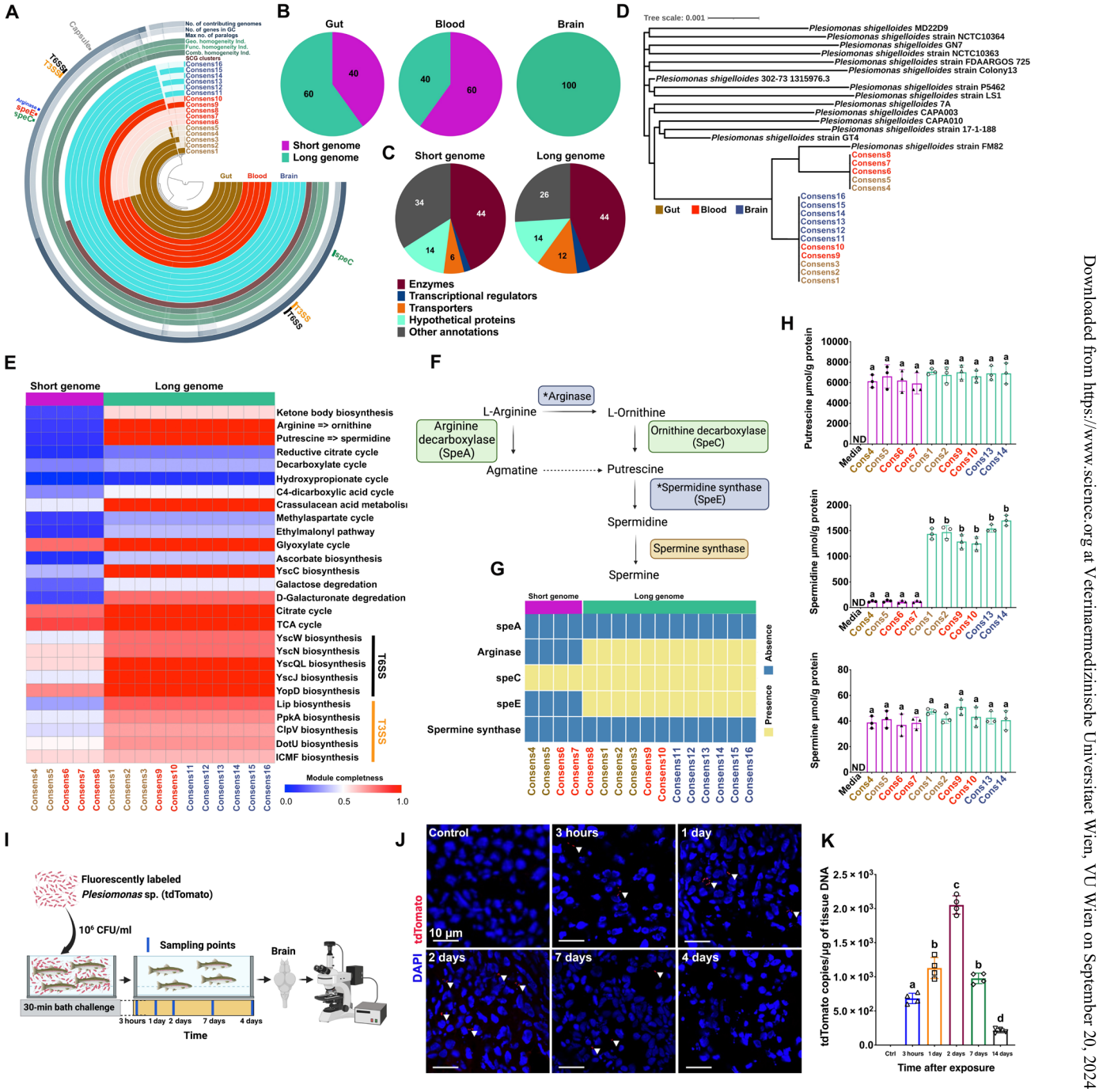

Fig. 3. Whole-genome sequencing (WGS) of brain-resident bacterial isolates suggests potential signatures of brain colonization and niche adaptation. (**A**) Pan-genome analysis of *Plesiomonas* sp. isolates from trout gut, blood, and brain. (**B**) Relative percentage of isolates with short and long genomes from each source (gut, blood, and brain). (**C**) Functional classes of annotated genes in short-genome and long-genome *Plesiomonas* sp. isolates. (**D**) Phylogenetic tree of *Plesiomonas* sp. isolates based on whole-genome data compared to publicly available strains. (**E**) Heatmap of module completeness for Kyoto Encyclopedia of Genes and Genomes pathways from *Plesiomonas* sp. genomes sequences in this study. (**F**) Bacterial polyamines synthesis pathway diagram. Asterisks in light purple boxes: genes missing in short-genome isolates; green boxes: genes encoding for enzymes found in all genomes; light orange box: genes encoding for enzymes not found in any of the genomes. ICMF, isobutyryl-CoA mutase fused. (**G**) Heatmap showing the presence or absence of genes that encode for the main enzymes involved in the polyamine synthesis pathway in each of the Plesiomonas genomes sequenced. (**H**) Polyamine levels in bacterial growth media, short-genome, and long-genome Plesiomonas isolates. ND, not detectable. Different letters indicate statistically significant differences ($P < 0.05$) by Tukey's post hoc test. (**I**) Experimental design for bath exposure of juvenile rainbow trout to tdTomato-labeled *Plesiomonas* sp. (**J**) Confocal microscopy images of rainbow trout brain cryosections from 3 hours to 14 days after bath exposure showing the presence of tdTomato-Plesiomonas (red, white arrowheads). Images from the OT are shown but bacteria were detected in all brain regions ($n = 3$). Cell nuclei were stained with DAPI. Scale bars, 10 µm. (**K**) Quantification of Tdtomato plasmid copies from rainbow trout whole brain from 3 hours to 14 days after exposure ($n = 4$). Different letters denote statistically significant differences ($P < 0.05$) by Welch's ANOVA test.

compared to non-brain isolates (fig. S6, E and F). In the gut and blood, all isolates were identical, and therefore, we called them rainbow trout-type strain *Agrobacterium* sp., whereas, in the brain, all isolates were named exoP mutants (fig. S6B). exoP mutants (Atu4049, exopolysaccharide polymerization/transport protein) contained 63 amino acid variants, but the rest of the genes in this module did not diverge among isolates (fig. S6F). The findings suggest that bacteria capable of colonizing the trout brain appear to use diverse strategies to adapt to this specialized niche. Further evidence for niche adaptation, such as using shotgun metagenomics, is needed at this point to uncover the whole array of strategies used by bacteria to colonize and persist in the salmonid brain.

Gut-resident bacteria can colonize and persist in the trout brain

Given that 6.2 to 22.7% of the diversity of the trout brain bacterial community can be explained from gut sources, we hypothesized that some gut bacterial species could penetrate and colonize the trout brain. We performed an in vivo bath exposure experiment in juvenile rainbow trout using a long-genome gut *Plesiomonas* sp. isolate fluorescently tagged with tdTomato (Fig. 3I). We detected tdTomato-*Plesiomonas* in all regions of the trout brain by confocal microscopy as early as 3 hours after exposure, and bacteria persisted at 1 and 2 days after exposure (Fig. 3J). We repeated the same experiment at longer postexposure times (7 and 14 days) to determine whether colonization occurs in the mid and long terms. We found long-genome tdTomato-*Plesiomonas* in all animals and brain regions after 7 days but bacteria could only be detected at low numbers after 14 days in one out of three animals examined (Fig. 3J). Using quantitative PCR (qPCR), we quantified relative tdTomato-*Plesiomonas* loads over time in total brain extracts from control and tdTomato-*Plesiomonas*–exposed animals (Fig. 3K). In agreement with our microscopy data, we were able to detect tdTomato copies in the brains of exposed animals as early as 3 hours. Levels continued to increase at 1 day and peaked at 2 days after exposure. By day 7, levels were comparable to those detected at day 1, and by day 14, although still detectable, bacterial loads were significantly lower than at 3 hours (Fig. 3K).

Combined, these results demonstrate short to mid-term colonization of bacteria in the trout brain by a gut resident *Plesiomonas* sp. isolate. Whether *Plesiomonas* sp. persists in the brain beyond 14 days remains to be investigated. Similarly, whether other gut-resident strains are capable of short incursions into the brain and what are the functional consequences of this phenomenon remain to be elucidated.

Geographical survey of brain microbiomes from different salmonid species

To extend our observations to other salmonid species and geographical locations, we sampled freshwater and saltwater Atlantic salmon (*Salmo salar*), Gila trout (*Oncorhynchus gilae*), European rainbow trout (*Oncorhynchus mykiss*), and Chinook salmon (*Oncorhynchus tshawytscha*), an anadromous native species of the Pacific Northwest. Sampling locations are shown in Fig. 4A.

We sampled Atlantic salmon (*S. salar*) from Norway either from freshwater or saltwater sources. In this sampling, we obtained gut, blood, OB, and Tel. In freshwater samples, Actinobacteria was the predominant phylum (65.7%) within the gut microbiome, while in saltwater samples, Firmicutes dominated (41.1%). In the blood, both Actinobacteria and Firmicutes were present at high relative frequencies, though Actinobacteria was more prominent in freshwater salmon (47.3%) and Firmicutes in saltwater salmon (45.1%) (Fig. 4B). The brain microbiome of Atlantic salmon presented a unique profile, distinct from the gut and blood microbiomes. Actinobacteria was consistently the dominant phylum in the brain, accounting for 80.3% in freshwater and 73.2% in saltwater salmon (Fig. 4B). Community composition at the family level, aloha diversity, and weighted UniFrac distances for all Atlantic salmon samples is shown in fig. S7 (A to F). No Mycoplasmataceae were detected in the microbial reads from the gut samples of freshwater Atlantic salmon (fig. S7A). However, Mycoplasmataceae were present at low abundances in the freshwater Atlantic salmon brain, accounting for 2.8% of the overall diversity in the OB and 2.9% in the Tel (fig. S7A). In contrast, Mycoplasmataceae were not detected in any of the saltwater Atlantic salmon samples (fig. S7B). SourceTracker2 analysis in freshwater Atlantic salmon predicted that 45.3% of ASVs present in the brain are of gut origin, while 39.8% are attributable to the blood (Fig. 4D). In saltwater salmon, gut and blood sources were estimated to represent 47.9 and 43.9% of the brain bacterial ASVs, respectively (Fig. 4D). Since we did not sample the spleens of these animals, SourceTracker2 analyses including the spleen as a source could not be performed.

Gila trout is a native endangered salmonid species of New Mexico that has undergone severe bottlenecks and genetic drifts through ecological challenges and habitat deterioration (*63*–*65*). At the phylum level, the Gila trout gut microbial community was predominantly dominated by Proteobacteria (53%) and Firmicutes (27.2%) (Fig. 4B). At the family level, Lactobacillaceae (particularly *Lactobacillus salivarius*) and Chromobacteriaceae were the primary constituents of the gut bacterial community (fig. S7G). In the blood and spleen, Proteobacteria families like Chromobacteriaceae and Betaproteobacteria were the most frequent taxa. We detected a significant proportion of Propionibacteria constituting 16.4% of the overall blood bacterial community (Fig. 4B and fig. S7G). In terms of the brain microbial composition, Actinobacteria from the Burkholderiaceae family and Proteobacteria from the Propionibacteriaceae family were the most abundant members of the Gila trout brain microbiome (Fig. 4B and fig. S7G). Mycoplasmataceae reads were detected in the gut (1.9%), blood (7.4%), and spleen (0.9%) of Gila trout (fig. S7G). The Gila trout brain also showed Mycoplasmataceae in all the surveyed regions with relative abundances of 2% in the OB, 9.1% in the Tel, 2.9% in the OT, and 6.8% in the Cer (fig. S7G). Compared to other salmonids, the alpha diversity of the Gila trout gut community was significantly higher than that of the other tissues sampled (fig. S7H and table S2) and weighted UniFrac distances were only significantly different between the gut, blood, and spleen and the four brain regions (fig. S7I). PCoA analysis showed some separation between microbial community structures between the gut, blood, and brain (Fig. 4C). This is consistent with the "internal microbiomes" being partly sourced from the gut. SourceTracker2 analysis predicted that in Gila trout, 18.1% of the Tel bacterial ASVs originate from the gut and 41.3% from the blood, leaving 40.6% to unknown sources (Fig. 4D). Similar to rainbow trout, tank water contributed a very small percentage of the brain reads (fig. S8B). If we included the spleen as a potential source, then SourceTraker2 predicted that 16.8% of the Gila trout Tel bacterial ASVs originate from the gut, 36.6% from the blood, and 9.9% from the spleen, leaving 40.1% to unknown sources (fig. S8B). The diversity of the unknown source category in each brain region is shown in file S3.

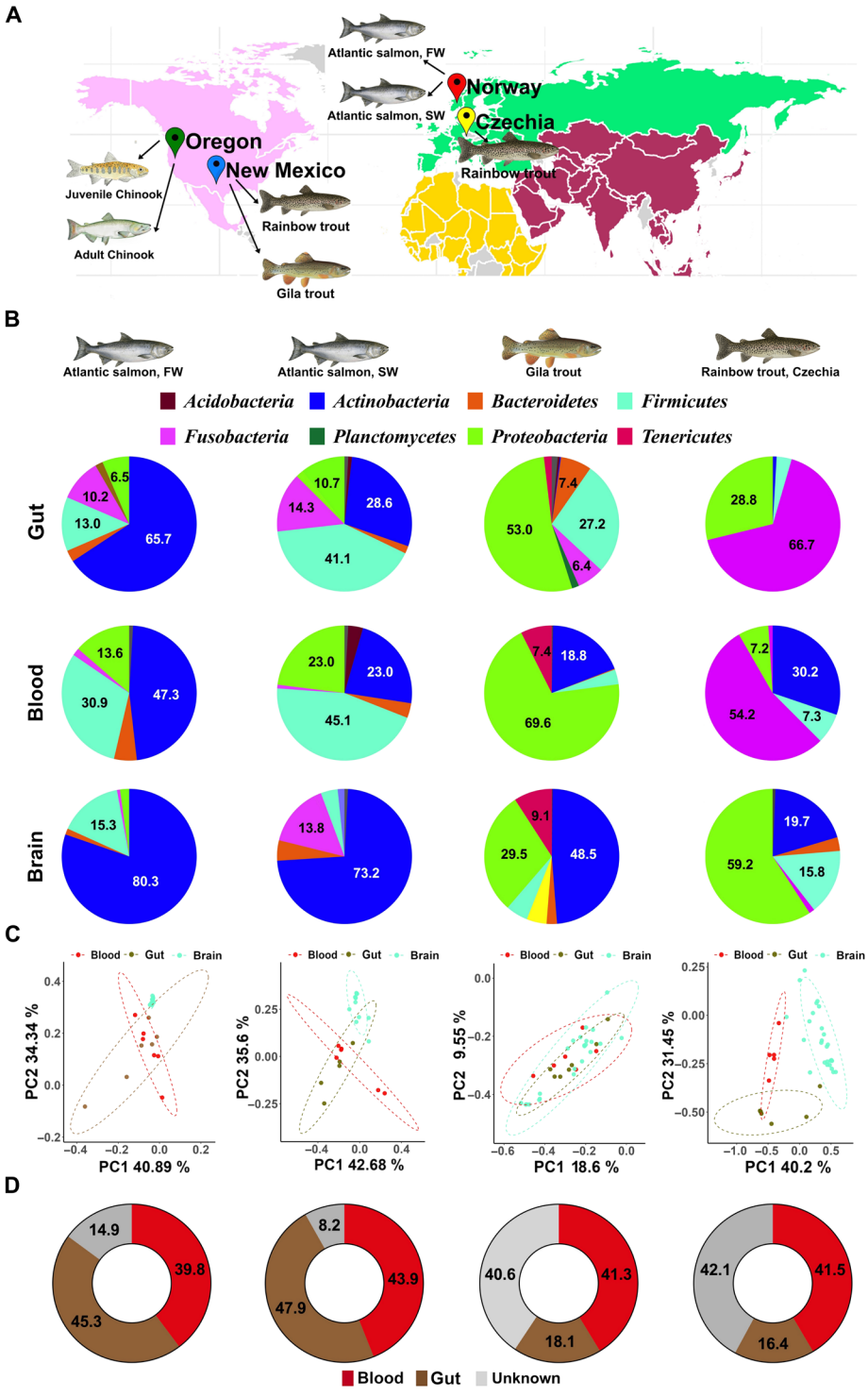

Fig. 4. Geographical survey of brain microbiomes from different salmonid species. (**A**) Map of the sampling locations and species sampled in this study ($n = 5$ to 7). Wild juvenile and adult Chinook salmon: Oregon, USA (September 2022); laboratory-reared rainbow trout and Gila trout: New Mexico, USA; Atlantic salmon (freshwater and saltwater phases): Norway; control laboratory rainbow trout: South Bohemia, Czechia. (**B**) Relative abundance of bacterial phyla present in the gut, blood, and brain (Tel) from freshwater Atlantic salmon, saltwater Atlantic salmon, Gila trout, and rainbow trout from Czechia. (**C**) PCoA illustrates the microbial community variations within the gut, blood, and brain across each salmonid group. Note that for Atlantic salmon, only Tel samples are included. Ellipses represent a 95% confidence interval, underscoring significant community composition differences ($P < 0.05$). (**D**) Relative contribution of gut and blood microbial communities as potential sources for bacterial communities in the brain (Tel) microbial community in each of the four salmonid groups predicted by microbial SourceTracker2 analysis.

We next sampled European rainbow trout from the Czech Republic, which offered an opportunity to compare their brain microbiome with that of our laboratory rainbow trout from the US. Our results indicate that the bacterial community composition of European rainbow trout was markedly different from the laboratory US rainbow trout. This was true for all body sites sampled. Notably, the gut bacterial community of the European specimens contained almost no *Mycoplasma* sp. (0.04%) (fig. S6J). No *Mycoplasma* reads were detected in the brain samples of the rainbow trout from Czechia. Similar to Atlantic salmon and rainbow trout from the US, the alpha diversity of the gut was significantly lower than that of all brain regions (fig. S7K), and the weighted UniFrac distance was greatest between the gut, blood, and spleen and the four brain regions (fig. S7L). In turn, the gut community was dominated by Fusobacteria (66.7%) and Proteobacteria (28.8%) (Fig. 4B). In the blood, Fusobacteria (66.7%) and Actinobacteria (30.2%) were the dominant phyla (Fig. 4B). The brain bacterial community was composed of Proteobacteria (32.8 to 72.3%), Actinobacteria (9.2 to 43.1%), and Firmicutes (15 to 22.6%) in different brain regions (Fig. 4B). SourceTracker2 analyses of the Czech Republic rainbow trout samples estimated that 16.4% of the Tel bacterial ASVs originate from the gut and 41.5% from the blood, leaving 42.1% to unknown sources (Fig. 4D). When the spleen was included as a source, we found that 9.7% of the Tel ASVs were predicted to originate from the spleen, while gut and blood accounted for 15.4 and 32.8% of the Tel ASVs respectively, leaving 42.1% to unknown sources (fig. S8C). The diversity of the unknown source category for each brain region is shown in file S3. A summary of alpha diversity and beta diversity metrics for all microbiome sequences generated in this study is shown in fig. S7 and table S2. Combined, our survey uncovered bacterial communities in the brains of all salmonid species sampled. Salmonid brain microbial communities appear to be largely determined by host genetics as well as the environment as is the case for microbial communities associated with mucosal barriers.

Brain microbiomes shift during the life cycle of Chinook salmon

Chinook salmon are anadromous salmonids with long, complex, and diverse life histories (*66*). This species has great cultural, economic, and ecological importance in the Pacific Northwest, and many populations are in decline. Understanding the role of the brain microbiome in Chinook salmon is therefore of interest to better understand their physiology and behavior. After spending approximately 8 to 16 months in their natal freshwater habitats (*67*), juveniles migrate downstream to the ocean where they spend 1 to 5 years before returning to estuaries and migrating to their natal streams, where they undergo final maturation, reproduce, and die (Fig. 5A) (*66*). The long migration up the river where they will spawn is accompanied by marked losses of body condition due to feeding cessation, elevated cortisol levels, lethargy, multi-organ damage, and neurodegeneration (*34*, *68*–*72*). After spawning, Chinook salmon die in a process known as reproductive death. Previous studies in Atlantic salmon from natural water bodies also captured critical shifts in the gut microbial community during its migratory life cycle (*73*), but shifts in internal microbiomes were not investigated. Given that Chinook salmon in the Willamette River develop severe intestinal lesions, inflammation, and loss of villar structure as they approach spawning (*74*, *75*), we hypothesized that leakiness from the gut compartment into the systemic compartment would cause alterations in their brain microbiome. Bacterial loads in the adult gut and blood were significantly higher than in juveniles, whereas the loads in the spleen did not show any differences. In the brain, bacterial loads were significantly higher in Tel and Cer for sexually mature animals compared to juvenile Chinook salmon (Fig. 5B). Microbiome analyses further supported the convergence of the brain, gut, and blood microbial community composition between adult and juvenile Chinook salmon as shown by PCoA (fig. S9, A to G). In support, endotoxin levels in the serum of reproductively mature Chinook salmon were threefold higher compared to juveniles (Fig. 5C). As predicted, compared to juveniles, mature Chinook salmon have signatures of pathogenic bacteria circulating in their blood including *Flavobacterium psychrophilum* and *Flavobacterium columnare* (Fig. 5, F and G). Furthermore, we detected greater abundances of Burkholderiaceae and Enterobacteriaceae within the brains of adult Chinook salmon (Fig. 5, F, G, and I). Conversely, juvenile Chinook salmon brains were predominantly characterized by the presence of Mycoplasmataceae (40% in the OB, 75.5% in the Tel, 39.6% in the OT, and 25.5% in the Cer) and Propionibacteriaceae (27.8% in the OB, 9.8% in the Tel, 15.3% in the OT, and 24.7% in the Cer) (Fig. 5, D to G). PCoA analysis of the microbial community composition of the Tel across all samples collected revealed that the greatest separation between communities was due to developmental stage (juvenile versus adult Chinook salmon), while the Tel microbial communities of both Atlantic salmon groups tightly clustered together and were closely related to both New Mexico sampling groups (rainbow trout and Gila trout) (Fig. 5H). A combined linear discriminant analysis of all the Tel microbial communities for all salmonid species and sampling conditions is shown in Fig. 5I. SourceTracker2 analyses revealed that the blood contributed to 34 to 41% of the brain communities in juvenile Chinook depending on the brain region, whereas in adults, these percentages ranged between 36 and 48% except for the Cer where it was only 18%. The gut, in turn, contributed to 34 to 45% of the brain microbial community in juveniles and 25 to 58% in adults depending on the brain region. The spleen was predicted to contribute between 8 and 12% to the brain microbial communities in both juveniles and adults (fig. S8, D and E). The diversity of the unknown source category in all Chinook salmon brain samples is shown in file S3. Since systemic inflammation is known to result in neuroinflammation and breakdown of the blood-brain barrier (*76*–*78*), our findings suggest that the homeostatic brain microbiome becomes disrupted toward the end of the maturation life cycle in Pacific salmon. Whether the changes in microbial signatures detected in adult Chinook salmon brains and blood contribute to the characteristic lethargy, altered swimming behavior (*79*), and neurological dysfunction (*80*) of mature Chinook salmon before reproductive death remains unclear.

Bacteria accumulate in the brain of mature adult Chinook salmon

Previous work in mammals suggests that beta amyloid plaques are an antimicrobial reaction in the brain (*81*–*83*). Salmonids such as Chinook salmon which undergo reproductive death accumulate beta amyloid in their brain and show signs of neurodegeneration (*72*, *84*, *85*). We therefore hypothesized that beta amyloid deposition in mature salmon may be associated with the penetration of bacteria into the brain. We stained the brains of juvenile and mature adult Chinook with anti-LPS and anti–beta amyloid antibodies. Whereas no beta amyloid and very little LPS signal could be detected in juvenile brains (Fig. 5J), LPS was abundant in the adult Chinook brain,

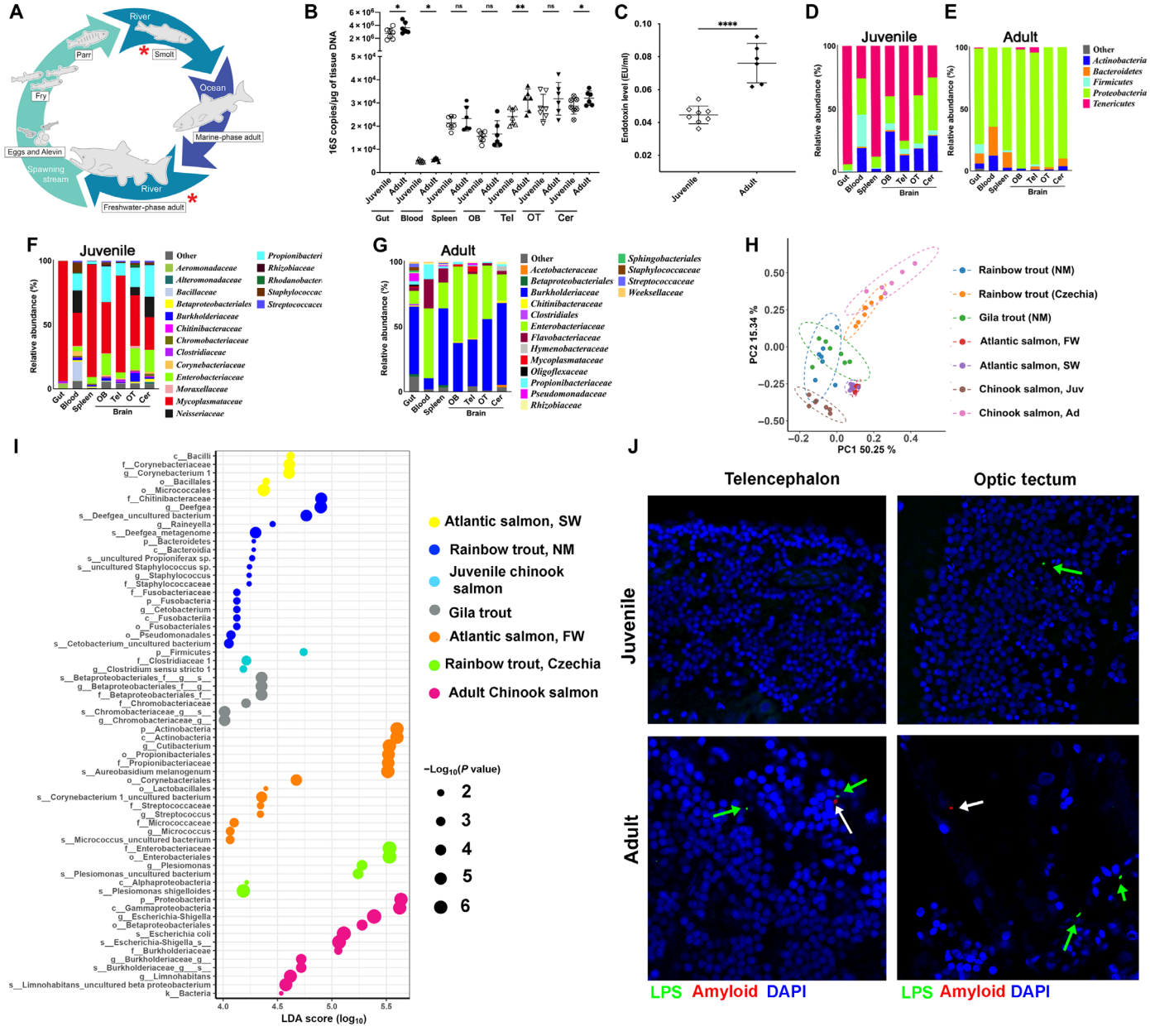

Fig. 5. Chinook salmon brain microbiomes shift during life cycle. (**A**) Schematic representation of the natural life cycle of Chinook salmon. Red asterisks indicate the two life stages sampled in this study. (**B**) Relative bacterial loads quantified by qPCR in the gut, blood, spleen, and four regions of the brain of juvenile and adult Chinook salmon. $*P < 0.05$; $**P < 0.01$ by Welch's ANOVA test. ns, not significant. (**C**) LPS levels in serum from juvenile and adult Chinook salmon, $****P < 0.0001$ by Tukey's post hoc test. (**D** and **E**) Bacterial community composition at the phylum level of the gut, blood, spleen, and four areas of the brain of juvenile (D) and adult (E) Chinook salmon. (**F**) Bacterial community composition at the family level of the gut, blood, spleen, and four areas of the brain of juvenile Chinook salmon. (**G**) Bacterial community composition at the family level of the gut, blood, spleen, and four areas of the brain of adult Chinook salmon. (**H**) PCoA of the weighted UniFrac distance of the brain (Tel only) bacterial communities of all salmonids sampled in this study. Ellipses represent a 95% confidence interval, underscoring significant community composition differences ($P < 0.05$). (**I**) Linear discrimination analysis of the brain (Tel only) bacterial communities of all salmonids sampled in this study. (**J**) Immunofluorescence staining of Tel and OT paraffin sections from juvenile and adult Chinook salmon with anti–*E. coli* LPS antibody (green) and anti–β amyloid (red) shows elevated LPS levels and the presence of β amyloid in adult Chinook brain tissues compared to juveniles ($n = 3$). Nuclei were stained with DAPI (blue). Green arrows indicate LPS-positive puncta and white arrows point at β amyloid–positive puncta.

supporting the 16*S* rDNA sequencing data. Furthermore, LPS was sometimes adjacent to beta amyloid–positive regions, especially in the OT (Fig. 5J). This finding suggests a potential association between bacterial dysregulation and beta amyloid accumulation in the brain of mature Chinook salmon, supporting previous findings in mammals.

DISCUSSION

Microorganisms shape the vertebrate brain via complex biological processes, the best characterized being the gut-brain axis (*1*–*3*). This bidirectional communication involves molecular mediators released by microorganisms but not direct microbial colonization of the brain. Our findings uncover remarkable associations between the

salmonid brain and bacteria during healthy physiological states. Whether this is a hallmark of other teleosts or a universal symbiotic relationship found in all vertebrates remains to be investigated.

Our study identifies several potential mechanisms by which bacteria can colonize the trout brain. First, our data suggest that brain bacteria are partly sourced from the gut and the blood and that bacteria appear to cross the blood-brain barrier and colonize the parenchyma in healthy rainbow trout without causing any disease. We also think that bacteria may reside intracellularly in different cell types within the brain, the type of the cells carrying bacteria is yet to be resolved. However, our efforts to perform cell segmentation in combination with in situ hybridization were not successful, and therefore, we will have to continue our work to ascertain the intracellular nature of brain bacteria in salmonids. In mammals, microbiota are found to reside within phagocytes (dendritic cells) in intestinal lymphoid tissues and mesenteric lymph nodes (*86*, *87*). Thus, it is plausible that phagocytes are reservoirs of some bacteria in the salmonid brain, a question that we hope to address in future studies.

Teleosts are highly resistant to endotoxin shock (*14*, *15*). Yet, similar to mammals, teleosts can also tolerate endotoxin. For instance, zebrafish embryos pre-exposed to sublethal LPS doses in the laboratory show reduced mortality to subsequent lethal exposures (*88*). Our work contributes to our understanding this phenomenon in a natural system. Specifically, the continuous presence of internal microbiomes in teleost fish may contribute to LPS tolerization throughout life and at physiological states.

A critical question that emerges from our work is how stable brain microbial communities are in salmonids. Some limitations of our study include the fact that we did not determine the duration of Plesiomonas colonization beyond 14 days and we did not quantify active replication of bacteria locally, once they enter the brain. Thus, it is unclear whether the symbiosis between the salmonid brain and microbiota is a long-lived, stable relationship or rather represents a dynamic, transient community that requires recurrent replenishment via the blood (and perhaps other sources) in a continuous fashion. Understanding these dynamics may shed light on broader questions regarding the microbiome's influence on teleost neurobiology as well as its role in modulating the brain's immune system. Similarly, the presence of bacteria in the spleen and blood of healthy teleosts suggests that microbiota may continuously and directly educate the systemic immune system in these species throughout their life span.

Our data suggests that some members of the salmonid brain bacterial community may acquire niche adaptations both in their genomes and their metabolic capabilities. While our efforts showcase brain niche adaptations of *Plesiomonas* sp. and *Agrobacterium* sp., microbial adaptations to brain niches likely occur in other taxa and span other metabolic functions yet to be found. Our study, in this sense, presents some important limitations, including the lack of shotgun metagenomics data, which would be necessary to fully resolve the niche adaptation question. Moreover, understanding the functional consequence of brain microbiomes in salmonids is a critical and nontrivial question to answer. While fish gnotobiotic systems exist (*89*–*93*), these systems remove microbiota from all mucosal surfaces, affecting brain form and function and behavior as previously reported by others. Thus, while useful, gnotobiotic systems would not fully answer the question of what functions these bacteria may play in the host brain. Coupling gnotobiotic systems with monocolonization experiments with bacterial isolates and laboratory mutants that cannot penetrate the brain will shed light on some of these questions.

Our work at homeostasis evidently raises questions as to how salmonid brain microbial communities are affected in different disease states and whether these communities contribute to diverse processes such as sickness behaviors, cognition, locomotion, or sensory perception. In summary, our findings demonstrate that microorganisms directly colonize the brain of salmonids, redefine the boundaries between microbiota and the healthy vertebrate brain, and may explain why teleosts are particularly tolerant to LPS.

MATERIALS AND METHODS

Animals

While all animals were monitored for health and appeared healthy during the study, it must be noted that adult Chinook salmon often exhibit opportunistic infections toward the end of their life cycle. This is likely due to increased stress and immunosuppression commonly observed in these fish as they approach reproductive death (*68*, *75*). Laboratory rainbow trout were obtained from Trout Lodge (Washington, USA) as 0.5-g larvae and maintained at the University of New Mexico Aquatic Animal Facility. Trout were maintained in a recirculating aquarium system at 16°C and under a 12L:12D photoperiod. Trout were fed commercial pelleted diets (Skretting, USA). Animals were sampled at a mean weight of 30 g unless otherwise stated. Gila trout (mean weight = 10 g) were obtained from the New Mexico Fish and Wildlife facility (Albuquerque, NM) and maintained at 10° to 12°C. All rainbow trout and Gila trout procedures were approved by the University of New Mexico Institutional Animal Care and Use Committee under protocol number 22-201239-MC.

Freshwater Atlantic salmon (*S. salar*) (mean weight = 60 g) were maintained in a recirculating system at 12°C at the Industrial and Aquatic Laboratory (ILAB) facility in Bergen, Norway. Seawater Atlantic salmon (mean weight = 150 g) were maintained in a flow-through system with 34–part-per-million (ppm) salinity at 9°C at the same facility. Fish were fed with standard feed from Skretting, with 2- and 3-mm-sized pellets, for freshwater and saltwater individuals, respectively. Animals were euthanized, bled, and perfused as described below.

Hatchery rainbow trout (mean weight = 120 g) from the Czech Republic were obtained from a recirculating aquarium system at University of South Bohemia. Trout were maintained at 16°C under a 12L:12D photoperiod and fed a commercial diet INICIO plus and EFICO Enviro 920 Advance (BioMar, Denmark). Animal procedures were performed in accordance with Czech legislation (section 29 of Act No. 246/1992 Coll. on the protection of animals against cruelty, as amended by Act No. 77/2004 Coll.) and approved by the Ministry of Education, Youth and Sport (MSMT-18301/2018-2).

Wild juvenile Chinook salmon were collected in September 2022 by the Oregon Department of Fisheries and Wildlife (ODFW) personnel from a screw trap on the North Santiam River near Stayton, Oregon, USA (latitude, 44.7960; longitude, −122.7792) under the auspices of a NOAA State 4(d) research permit (#26225). Fish were euthanized using 200-ppm tricaine methanesulfonate (MS-222) before dissection and tissue sampling. Fresh adult Chinook salmon carcasses were obtained from an ODFW hatchery and sampled on-site. These fish were trapped in June 2022 during their migration up the Willamette River, treated prophylactically with oxytetracycline to prevent bacterial diseases, and transported to holding ponds

at Willamette Hatchery near Oakridge, Oregon, USA (latitude, 43.9249; longitude, −122.8078) for use as brood fish. Adults were held until mid-September when they were humanely euthanized and artificially spawned for propagation by ODFW employees. Blood and tissues were sampled immediately after euthanasia. All Chinook salmon sampling was approved by Oregon State University Institutional Animal Care and Use Committee (ACUP #2020-0119).

Tissue sampling and aseptic techniques

Animals ($n = 7$ per species) were euthanized with MS-222 (200 ppm, Syndel), and aseptic techniques were strictly followed to collect all samples. Rigorous procedures were implemented to eliminate the possibility of any microbial contamination in brain samples. Before sampling, all incision sites or needle entry points were disinfected using bleach, followed by 80% ethanol disinfection using soaked Kimwipes. To ensure sterile conditions, sampling of rainbow trout in New Mexico as well as Gila trout was conducted in a laminar flow hood. Before sampling, the hood was cleaned using a PREempt spray, followed by two rounds of 80% ethanol cleaning. Next, autoclaved dissecting tools, dissection trays, and tubes were placed within the hood and subjected to 1 hour of ultraviolet (UV) exposure. For all other geographical samplings, we maintained sterile conditions by autoclaving all the dissection tools, tubes, and reagents, disinfecting all the surfaces including tables and dissection trays by PREempt spray and two rounds of 80% ethanol cleaning. In this case, sampling was done next to a Bunsen burner since we did not have access to laminar flow hoods or UV disinfection. We included technical controls for all samples and sampling locations.

Following blood collection from the caudal vein, a thorough perfusion with 10 ml of sterile phosphate-buffered saline (PBS) was conducted to clear any remaining blood from the tissues. To guarantee no recirculation toward the brain, branchial arch veins and the caudal vein were severed before perfusion, enabling a unidirectional flow from the heart to the brain. Autoclaved tools were used to collect each tissue sample from the midgut, blood, spleen, and specific brain regions: OB, Tel, OT, and Cer. All collected samples were immediately placed in 1 ml of sucrose lysis buffer and preserved at −80°C for subsequent processing for all species except for Atlantic salmon where only midgut, blood, OB, and Tel were sampled. Any remaining fecal contents were removed during the dissection process before the collection of the midgut samples. Negative controls were included at every stage of the procedure as recommended for low biomass microbiome sequencing (*17*, *94*). Specifically, we included three control tubes containing sucrose lysis buffer (SLB) which were left with their caps open on the same rack as the experimental samples during the sampling procedure. These negative controls were included in every sampling and processed for DNA extraction in the same way as all experimental samples. During transport from Europe to the US, temperature was monitored to ensure that all samples stayed at −80°C.

Perfusion efficiency

To measure the perfusion efficiency, we quantified the residual hemoglobin levels in the gut, spleen, and brain of non-perfused and perfused trout ($n = 4$). Tissues were first subjected to mechanical lysis in glass beads using 1 ml of sterile PBS in a TissueLyser II (Qiagen) set at 30 oscillations per second for 5 min. Subsequently, the lysates were centrifuged at 1000 rpm for 1 min. Two hundred microliters of each supernatant was used for the quantitative analysis of hemoglobin levels using a standard curve generated from bovine hemoglobin. Absorbance at 415 nm was measured in an iMark microplate reader (Bio-Rad), as previously described (*95*).

Antibiotic gavage

Rainbow trout ($n = 4$ per group) were orally gavaged with 100 μl of an antibiotic cocktail daily for 7 days using a plastic tubing gavage needle (GavageNeedle, USA). The cocktail consisted of ampicillin (10 mg/kg; Thermo Fisher Scientific), metronidazole (10 mg/kg; Thermo Fisher Scientific), neomycin (20 mg/kg; Sigma-Aldrich), tetracycline (20 mg/kg; VWR), and vancomycin (10 mg/kg; Combi-Blocks, CA, USA), all diluted in PBS. This selection was based on prior in vivo studies in mice (*96*, *97*). Controls were gavaged with the same volume of PBS every day for 7 days. Animals were sampled 1 day after the last gavage dose. No mortalities were recorded during the duration of the experiment.

Culturomics and colony-forming unit quantification in tissues

Midgut, blood, spleen, OB, Tel, OT, and Cer were collected from a total of eight rainbow trout, which were divided into two groups based on the lysis method applied. Fecal content was removed from the gut before tissue collection. Rigorous aseptic techniques were meticulously adhered to during the sampling process, as explained above and as previously described (*98*). Negative controls consisting of plates that were opened and closed next to the flame but without inoculum were also included. Environmental controls consisted of 10 cm–by–10 cm swabs from the laboratory benches (fig. S2D) and the laminar flow hood (fig. S2E) ($n = 3$ each), both before and after implementing described disinfection procedures. Swabs were placed in 100 μl of sterile PBS and plated under the same conditions as the tissue samples. For mechanical lysis, tissues were placed in 300 μl of sterile PBS containing sterile glass beads and mechanically lysed at a frequency of 20 shakes per second for 3 min in a TissueLyser II (Qiagen). Negative controls consisted of tubes containing PBS and beads but no sample. The second set of samples was placed in a tissue lysis buffer consisting of 0.05% NP-40 in PBS to which sterile glass beads were also added, and the tubes were treated for the mechanical lysis (*98*). Lysates were then centrifuged at 1000 rpm for 1 min, and 30 μl of the lysate supernatant was used for culturing under different conditions. We tested LB, NB, TSB, and MacConkey and Mycoplasma growth media. All expansion cultures, in conjunction with the plates corresponding to each specimen, were consistently maintained at three distinct temperatures: 16°C, ambient room temperature (25°C), and 30°C. Unique bacterial colonies exhibiting distinct morphologies were selected from each plate and then subjected to 16*S* rDNA sequencing for bacterial identification, as explained in (*98*).

DNA extraction and 16*S* rDNA library preparation

Initial lysis was achieved using two tungsten carbide beads for each tube and subsequently agitated using the Qiagen TissueLyser II for 5 min at a frequency of 30 shakes per second. Following mechanical lysis, 200 μl of 1% CTAB (hexadecyltrimethylammonium bromide; Sigma-Aldrich) and 3 μl of proteinase K (100 mg/ml) were added to each sample. DNA extractions were performed as described before by Mitchell and Takacs-Vesbach (*99*). The integrity and concentration of the DNA for each sample were measured in a NanoDrop ND-1000 spectrophotometer. Depending on the primary

concentration, DNA samples underwent dilutions of either 1:10 or 1:20 to use as templates.

Negative and positive controls were included in all our library preparations as recommended by the microbiome research community (*17*, *94*). The DNA template for each PCR reaction was standardized to a minimum of 200 ng to reduce the impact of potential contaminants. Although negative controls did not reach this concentration, the product from the DNA extraction step was subjected to PCR amplification. Each sample was run in triplicate PCR reactions, and the products were pooled before cleaning and library preparation. In each library run, a positive control containing DNA from seven known bacterial species grown in the laboratory was included to benchmark sequencing fidelity. An additional control consisting of a mouse colon sample was included in each run to assess consistency across the sequencing runs.

For each sample, three separate PCR reactions were carried out on each sample to amplify the V1 to V3 regions of the prokaryotic 16*S* rDNA, using the primers 28F (sequence: 5′-GAGTTTGATCNTGGCTCAG-3′) and 519R (sequence: 5′-GTNTTACNGCGGCKGCTG-3′) as explained before (*27*). Amplification products for each sample were then pooled and purified by AxyPrep Mag PCR Clean-up Kit (Thermo Fisher Scientific). PCR amplicons were then barcoded using the Nextera XT Index Kit v2 Sets A, B, C, and D (Illumina). Amplicon concentration across samples was normalized to 200 ng/μl using the Qubit High Sensitivity dsDNA assay before pooling. The library was subject to an additional round of purification using the Axygen PCR clean-up kit. Libraries were sequenced in an Illumina NextSeq 2000 platform using the Illumina NextSeq 2000 Reagent Kit (600 cycles) at the Clinical and Translational Sciences Center at the University of New Mexico Health Sciences Center.

Microbiome data analyses

Sequences were processed using the Quantitative Insights Into Microbial Ecology 2 (Qiime2, v2023.7) pipeline (*100*). The Divisive Amplicon Denoising Algorithm (DADA2) was used to cluster demultiplexed sequence reads into ASVs (*101*). ASVs were subsequently aligned to the SILVA 16*S* rDNA database (v138) for taxonomic classification (*102*). Before the core diversity analyses, each sample was standardized to a depth of 3500 reads, which was sufficient to reach rarefaction. A subsequent core diversity analysis factored both temporal and treatment variables. Indices of alpha diversity (Shannon diversity, Chao1, Faith's PD) and measures of beta diversity (weighted UniFrac distances) were generated in QIIME2. Beta diversity metrics ordination was visualized with PCoA plots, constructed using the Qiime2R package in RStudio version 1.3.959 (*103*). Using the SourceTracker2 plugin within the QIIME2 framework (*104*), we subjected the 16*S* rDNA sequences from the spleen, OB, Tel, OT, and Cer as sinks and the gut, blood, and water (in the case of rainbow trout and Gila trout) were used as presumptive sources for the observed ASVs in each cohort. In addition, we performed separate analyses, including the spleen along with the gut and blood as sources for the OB, Tel, OT, and Cer (sinks). Squeegee (*105*) was used to identify any potential microbial contamination in brain samples.

Bacterial load quantification

Bacterial loads in each specimen were measured by using quantitative PCR for the 16*S* rDNA as described (*106*). The process involved amplifying the bacterial 16*S* rDNA sequences in triplicate, using primers that were designed to anneal to the V1 to V3 variable regions, as previously described (*27*). The reaction setup for qPCR was composed in a 96-well plate with 2 μl of normalized DNA/cDNA of 10 ng/μl, 2 μl of primers mix, 6 μl of nuclease-free water, and 10 μl of SsoAdvanced Universal SYBR Green supermix (Bio-Rad). The amplification protocol started with an enzyme activation at 94°C for 90 s, followed by 33 cycles of denaturation at 94°C for 30 s, annealing at 52°C for 30 s, extension at 72°C for 90 s, and concluded with a final extension at 72°C for 7 min and a stabilization at 4°C (*27*) in a Bio-Rad CFX96 C1000 Touch system. The quantification of the 16*S* rDNA copies in the samples was calculated against a standard curve derived from a serial dilution of *Escherichia coli* 16*S* rDNA gene copies, ranging from 10^9 to 10 copies for the V1 to V3 regions. Negative controls were included in all PCR plates.

In situ hybridization and confocal microscopy

Cryo-mounted fish heads were sectioned to 10 μm thickness using the LEICA CM3050-s cryosectioning machine. Before sectioning, a meticulous decontamination process was executed wherein all brushes and surfaces of the cryosectioning equipment underwent a primary treatment with a 10% bleach solution, followed by dual treatments of absolute ethanol. Following sectioning, brain sections were fixed in a 4% paraformaldehyde (PFA) solution for 10 min. Following an overnight permeabilization step in 70% ethanol in diethyl pyrocarbonate water, samples were then hybridized using Cy5-labeled EUB338 (5′[Cy5]GCTGCCTCCCGTAGGAGT-3′) or Cy5-labeled NONEUB as technical negative control (5′[Cy5]ACTCCTACGGGAGGCAGC-3′) (Eurofins Genomics). We also used the Cy3-labeled Mycoplasma probe (5′[Cy3]GTGGCGAACGGGTGAGT3′) or Cy3-labeled NON-Mycoplasma probe as a technical negative control (5′[Cy3]ACTCACCCGTTCFCCAC3′) (Eurofins Genomics). Probes (3 μg/ml) were added to a hybridization buffer containing 2× SSC integrated with 20% formamide (Thermo Fisher Scientific). Hybridization was performed by incubating the slides at 45°C overnight. After washing the slides with a probe-free hybridization medium, two other washes in PBS were performed. Nuclei were stained with 4′,6-diamidino-2-phenylindole (DAPI; 1 μg/ml) for 30 min at 37°C (Invitrogen). In addition, some slides were stained with a solution containing DAPI (1 μg/ml) and 0.1 μM Alexa Fluor 555–phalloidin (Thermo Fisher Scientific) to label F-actin. Slides were mounted in Fluoroshield medium (Sigma-Aldrich) and imaged on a Zeiss LSM 780 or a Zeiss LSM 800 confocal microscope with ZEN microscopy software version 3.3.

Bacterial whole-genome sequencing (WGS), assembly, annotation, and pan-genome analyses

To sequence the genomic profiles of the bacterial isolates outlined in table S3, we cultured each isolate using their respective media and temperature conditions, as delineated in table S7, for 24 hours. High–molecular weight DNA from the bacterial pellets was extracted with the QIAGEN DNeasy Blood and Tissue Kit. For consistency, we standardized the DNA extracts to a concentration of 50 ng/μl, as measured by the Qubit High Sensitivity dsDNA assay. A 25-μl aliquot of each DNA preparation was sent to Plasmidsaurus (OR, USA) for Oxford Nanopore sequencing. Upon retrieval of the raw FASTq reads, we used PycoQC version 2.5.2 to ensure quality assurance (*107*). De novo genome assembly for each sample was performed in Shasta version 0.11.1 (*108*). All the sequenced genomes showed a sequencing coverage of at least 40×. Assembled genomic scaffolds exceeding 500 bp were subjected to a rigorous annotation regimen through Prokka (*109*) and FAMSA (*110*). Pan-genome analysis was conducted and visualized using Anvi'o, version 7.1 (*111*).

Phylogenetic trees were constructed using IQ-TREE (*112*), and KEGG metabolic reconstructions were performed in Anvi'o, version 7.1 (*111*).

Bacterial fluorescent tagging and immersion experiments

Plesiomonas sp. bacteria, tagged with tdTomato, were cultured in tryptic soy broth supplemented with 1% NaCl. The specific strain of Plesiomonas was a gut isolate with a long genome (table S5, consens2) isolated from laboratory rainbow trout at the University of New Mexico. After labeling, we resequenced the genome to ensure that there was no contamination during the labeling process. Bacteria were grown to an OD = 1.0. Rainbow trout (mean weight = 3 g) were exposed to aquarium water containing 10^6 CFUs/ml of tdT *Plesiomonas* sp. for 30 min at 18°C under gentle aeration. Control animals were subject to the same immersion treatment with aquarium water without bacteria. Trout ($n = 4$ per time point) were sampled 3 hours, 1 day, 2 days, 7 days, and 14 days after immersion. All fish were perfused with sterile PBS to remove residual blood from the vasculature. Immediately after sampling, fish heads were embedded in a cryomounting medium, and a rapid freezing process was initiated using liquid nitrogen. All solutions used during tissue processing were prepared with nuclease-free water to prevent potential RNA-DNA degradation. Cryosections ($n = 3$ fish per group) (10 μm) were fixed for 5 min in 4% PFA followed by two PBS washes each for 3 min. Nuclei were stained with DAPI solution (1 μg/ml; Invitrogen), and slices were mounted with Fluoroshield (Sigma-Aldrich). To quantify the presence of fluorescently tagged bacteria (Tdtomato-*Plesiomonas*) within the brain at each sampling point ($n = 4$), we used qPCR targeting the plasmid-encoded Tdtomato gene. The specific sequences of the primers used were as follows: the forward primer, 5′-CTGTTCCTGTACGGCATCG-3′ and the reverse primer, 5′-TCTTTGATGACGGCCATGT-3′. The qPCR reactions were performed with an annealing temperature of 62°C. Quantification of bacterial loads was achieved by comparing the Ct values of the samples to a preestablished standard curve derived from known concentrations of serially diluted Tdtomato-tagged *Plesiomonas* sp.

Serum LPS levels in juvenile and mature Chinook salmon

Blood serum samples were initially diluted 1:20 in endotoxin-free PBS (Millipore). Subsequently, this diluted mixture was incubated at 70°C for 15 min. Following the heat treatment, the quantification of endotoxin levels within these samples was conducted using the Chromogenic Endotoxin Quantification Kit (Pierce), as per the manufacturer's instructions. To ensure the elimination of potential pyrogenic contamination, all consumables used in the assay, including pipette tips, tubes, and microplates, were certified as nonpyrogenic.

Bacterial polyamine ELISA assays

Pure cultures of bacterial isolates were incubated in TSB medium for 24 hours, after which the bacterial cells were collected by centrifugation at 5500*g* for 20 min. The cell pellet was subsequently lysed using 1% Triton X-100 (v/v) (Sigma-Aldrich), as described (*113*). The polyamine profile of each isolate, including putrescine, spermidine, and spermine levels, was quantified using commercially available ELISA kits (MyBioSource) following the manufacturer's instructions.

Blood glucose tests

Following the collection of blood samples, the blood glucose was measured immediately. This was carried out using a TrueMetrix self-monitoring blood glucose meter. A single drop of blood obtained from each sample was applied to TrueMetrix blood glucose test strips, which were then read by the meter to give an instant measurement of blood glucose levels.

Chinook salmon brain immunofluorescence staining

Ten-micrometer-thick paraffin sections from juvenile and adult Chinook salmon brains ($n = 3$ per group) were deparaffinized and treated with trypsin antigen retrieval solution (Abcam, ab970) at room temperature for 15 min. After rinsing in PBS for 5 min at room temperature, sections were permeabilized in PBT (PBS with 0.1% Triton X-100) for 10 min at room temperature. Next, the sections were blocked in PBS/0.1% Tween 20 with 1% bovine serum albumin (BSA) for 30 min at room temperature with agitation. After blocking, the samples were incubated in Anti–*E. coli* LPS antibody [2D7/1] (ab35654) at 1:200 and recombinant Alexa Fluor 647 Anti–beta Amyloid 1-42 antibody [mOC64] (ab300742) at 1:150, both in PBS/0.1% Tween 20 with 1% BSA overnight at 4°C. On day 2, the sections were rinsed three times with PBS for 5 min each at room temperature with agitation. Next, the sections were incubated in goat anti-mouse IgG H&L (Alexa Fluor 488) (ab150113) at 1:300 in PBS/0.1% Tween 20 with 1% BSA for 1 hour at room temperature with agitation. The sections were then rinsed three times in PBS for 5 min each at room temperature with agitation. Then, the sections were incubated in DAPI at 1:500 in tap water for 2 min, rinsed, and mounted with KPL fluorescent mounting media. Slides were imaged with a Zeiss LSM 780 confocal microscope using the Zen software.

Statistical analyses

For the quantification of endotoxin levels in the blood serum across various fish groups, data were initially checked for normal distribution using both the *F* test and Bartlett's test. Differences between groups were assessed using a one-way analysis of variance (ANOVA) followed by Tukey's post hoc test. Bacterial loads, as quantified by 16*S* gene copies across different tissues, were subjected to the same normality checks. To discern variations among the different tissues and between groups, Brown-Forsythe and Welch's ANOVA test was used. For the microbiome Shannon diversity data, normal distribution checks were first conducted as described. Given the nonparametric nature of the data, a Kruskal-Wallis test was applied to determine differences among groups. In case of significant differences, post hoc pairwise comparisons were conducted with appropriate corrections for multiple testing. Weighted UniFrac distances were visually interpreted using PCoA plots. Differences in clustering on these plots across groups were tested for significance using the multivariate dispersion analysis. The data derived from SourceTracker2, representing percentages of various sources, and the module completeness percentages obtained from Anvi'o KEGG pathways were first subjected to the Shapiro-Wilk test to assess their distribution for normality. Following this, to investigate the differences between distinct groups, we used the Mann-Whitney *U* test for post hoc analyses. Significance in the presence or absence of specific genes or pathways in the pan-genome analysis was evaluated using Fisher's exact test. All statistical analyses were conducted using the GraphPad Prism (V10.0.3) and RStudio (R 4.2.3). Differences were considered statistically significant when $P < 0.05$.

Supplementary Materials

This PDF file includes:

Figs. S1 to S9
Tables S1 to S7
Data S1 to S3

REFERENCES AND NOTES

1. J. F. Cryan, K. J. O'Riordan, C. S. Cowan, K. V. Sandhu, T. F. Bastiaanssen, M. Boehme, M. G. Codagnone, S. Cussotto, C. Fulling, A. V. Golubeva, The microbiota-gut-brain axis. *Physiol. Rev.* **99**, 1877–2013 (2019).
2. K. J. O'Riordan, M. K. Collins, G. M. Moloney, E. G. Knox, M. R. Aburto, C. Fülling, S. J. Morley, G. Clarke, H. Schellekens, J. F. Cryan, Short chain fatty acids: Microbial metabolites for gut-brain axis signalling. *Mol. Cell. Endocrinol.* **546**, 111572 (2022).
3. L. Mohanta, B. C. Das, M. Patri, Microbial communities modulating brain functioning and behaviors in zebrafish: A mechanistic approach. *Microb. Pathog.* **145**, 104251 (2020).
4. R. D. Berg, Translocation of indigenous bacteria from the intestinal tract, in *Human Intestinal Microflora in Health and Disease* (Academic Press, 1983), chap. 15, pp. 333–352.
5. N. Geva-Zatorsky, E. Sefik, L. Kua, L. Pasman, T. G. Tan, A. Ortiz-Lopez, T. B. Yanortsang, L. Yang, R. Jupp, D. Mathis, Mining the human gut microbiota for immunomodulatory organisms. *Cell* **168**, 928–943.e11 (2017).
6. A. C. McPherson, S. P. Pandey, M. J. Bender, M. Meisel, Systemic immunoregulatory consequences of gut commensal translocation. *Trends Immunol.* **42**, 137–150 (2021).
7. Z. Hu, C.-A. McKenzie, C. Smith, J. G. Haas, R. Lathe, The remarkable complexity of the brain microbiome in health and disease. bioRxiv 2023.02.06.527297 (2023). https://doi.org/10.1101/2023.02.06.527297.
8. W. G. Branton, K. K. Ellestad, F. Maingat, B. M. Wheatley, E. Rud, R. L. Warren, R. A. Holt, M. G. Surette, C. Power, Brain microbial populations in HIV/AIDS: α-Proteobacteria predominate independent of host immune status. *PLOS ONE* **8**, e54673–e54673 (2013).
9. M. Prudencio, V. V. Belzil, R. Batra, C. A. Ross, T. F. Gendron, L. J. Pregent, M. E. Murray, K. K. Overstreet, A. E. Piazza-Johnston, P. Desaro, Distinct brain transcriptome profiles in C9orf72-associated and sporadic ALS. *Nat. Neurosci.* **18**, 1175–1182 (2015).
10. R. Alonso, D. Pisa, A. M. Fernández-Fernández, L. Carrasco, Infection of fungi and bacteria in brain tissue from elderly persons and patients with Alzheimer's disease. *Front. Aging Neurosci.* **10**, 159 (2018).
11. G. L. Bullock, S. F. Snieszko, Bacteria in blood and kidney of apparently healthy hatchery trout. *Trans. Am. Fish. Soc.* **98**, 268–271 (1969).
12. T. Ofek, M. Lalzar, I. Izhaki, M. Halpern, Intestine and spleen microbiota composition in healthy and diseased tilapia. *Anim. Microbiome* **4**, 50 (2022).
13. F. Fronton, S. Ferchiou, F. Caza, R. Villemur, D. Robert, Y. St-Pierre, Insights into the circulating microbiome of Atlantic and Greenland halibut populations: The role of species-specific and environmental factors. *Sci. Rep.* **13**, 5971 (2023).
14. I. Berczi, L. Bertok, T. Bereznai, Comparative studies on the toxicity of *Escherichia coli* lipopolysaccharide endotoxin in various animal species. *Can. J. Microbiol.* **12**, 1070–1071 (1966).
15. G. Wedemeyer, A. J. Ross, L. Smith, Some metabolic effects of bacterial endotoxins in salmonid fishes. *J. Fish. Board Can.* **26**, 115–122 (1969).
16. C. D. Link, Is there a brain microbiome? *Neurosci. Insights* **16**, doi. org/10.1177/26331055211018709 (2021).
17. R. Eisenhofer, J. J. Minich, C. Marotz, A. Cooper, R. Knight, L. S. Weyrich, Contamination in low microbial biomass microbiome studies: Issues and recommendations. *Trends Microbiol.* **27**, 105–117 (2019).
18. S. Mangul, H. T. Yang, N. Strauli, F. Gruhl, H. T. Porath, K. Hsieh, L. Chen, T. Daley, S. Christenson, A. Wesolowska-Andersen, ROP: Dumpster diving in RNA-sequencing to find the source of 1 trillion reads across diverse adult human tissues. *Genome Biol.* **19**, 36 (2018).
19. R. W. Lusk, Diverse and widespread contamination evident in the unmapped depths of high throughput sequencing data. *PLOS ONE* **9**, e110808 (2014).
20. M. L. Elkjaer, L. Simon, T. Frisch, L.-M. Bente, T. Kacprowski, M. Thomassen, R. Reynolds, J. Baumbach, R. Röttger, Z. Illes, Hypothesis of a potential BrainBiota and its relation to CNS autoimmune inflammation. *Front. Immunol.* **13**, 1043579 (2022).
21. J. A. Rasmussen, K. R. Villumsen, D. A. Duchêne, L. C. Puetz, T. O. Delmont, H. Sveier, L. von Gersdorff Jørgensen, K. Præbel, M. D. Martin, A. M. Bojesen, M. T. P. Gilbert, K. Kristiansen, M. T. Limborg, Genome-resolved metagenomics suggests a mutualistic relationship between Mycoplasma and salmonid hosts. *Commun. Biol.* **4**, 579 (2021).
22. J. Wang, Y. Li, A. Jaramillo-Torres, O. Einen, J. V. Jakobsen, Å. Krogdahl, T. M. Kortner, Exploring gut microbiota in adult Atlantic salmon (*Salmo salar* L.): Associations with gut health and dietary prebiotics. *Anim. Microbiome* **5**, 47 (2023).
23. J. A. Rasmussen, P. Kiilerich, A. S. Madhun, R. Waagbø, E.-J. R. Lock, L. Madsen, M. T. P. Gilbert, K. Kristiansen, M. T. Limborg, Co-diversification of an intestinal Mycoplasma and its salmonid host. *ISME J.* **17**, 682–692 (2023).
24. D. Bozzi, J. A. Rasmussen, C. Carøe, H. Sveier, K. Nordøy, M. T. P. Gilbert, M. T. Limborg, Salmon gut microbiota correlates with disease infection status: Potential for monitoring health in farmed animals. *Anim. Microbiome* **3**, 30 (2021).
25. Y. Jin, I. L. Angell, S. R. Sandve, L. G. Snipen, Y. Olsen, K. Rudi, Atlantic salmon raised with diets low in long-chain polyunsaturated n-3 fatty acids in freshwater have a Mycoplasma-dominated gut microbiota at sea. *Aquac. Environ. Interact.* **11**, 31–39 (2019).
26. L. Lowrey, D. C. Woodhams, L. Tacchi, I. Salinas, Topographical mapping of the rainbow trout (*Oncorhynchus mykiss*) microbiome reveals a diverse bacterial community with antifungal properties in the skin. *Appl. Environ. Microbiol.* **81**, 6915–6925 (2015).
27. Y. Ding, A. Fernandez-Montero, A. Mani, E. Casadei, Y. Shibasaki, F. Takizawa, R. Miyazawa, I. Salinas, J. O. Sunyer, Secretory IgM (sIgM) is an ancient master regulator of microbiota homeostasis and metabolism. bioRxiv 2023.02.26.530119 (2023). https://doi. org/10.1101/2023.02.26.530119.
28. R. M. Brown, G. D. Wiens, I. Salinas, Analysis of the gut and gill microbiome of resistant and susceptible lines of rainbow trout (*Oncorhynchus mykiss*). *Fish Shellfish Immunol.* **86**, 497–506 (2019).
29. P. P. Lyons, J. F. Turnbull, K. A. Dawson, M. Crumlish, Phylogenetic and functional characterization of the distal intestinal microbiome of rainbow trout *Oncorhynchus mykiss* from both farm and aquarium settings. *J. Appl. Microbiol.* **122**, 347–363 (2017).
30. C. Udoye, "Analytical challenges and characterization of skin and gut microbiota of Atlantic salmon fry in a commercial smolt production facility," thesis, Norwegian University of Science and Technology, 2018).
31. L. T. Lowrey, "The microbiome of rainbow trout (*Oncorhynchus mykiss*)," thesis, University of New Mexico (2014).
32. C. E. Dehler, C. J. Secombes, S. A. M. Martin, Environmental and physiological factors shape the gut microbiota of Atlantic salmon parr (*Salmo salar* L.). *Aquaculture* **467**, 149–157 (2017).
33. S. Ferchiou, F. Caza, R. Villemur, J. Labonne, Y. St-Pierre, Skin and blood microbial signatures of sedentary and migratory trout (*Salmo trutta*) of the Kerguelen Islands. *Fishes* **8**, 174 (2023).
34. C. E. Couch, W. T. Neal, C. L. Herron, M. L. Kent, C. B. Schreck, J. T. Peterson, Gut microbiome composition associates with corticosteroid treatment, morbidity, and senescence in Chinook salmon (*Oncorhynchus tshawytscha*). *Sci. Rep.* **13**, 2567 (2023).
35. H. A. Penny, R. G. Domingues, M. Z. Krauss, F. Melo-Gonzalez, M. A. E. Lawson, S. Dickson, J. Parkinson, M. Hurry, C. Purse, E. Jegham, Rhythmicity of intestinal IgA responses confers oscillatory commensal microbiota mutualism. *Sci. Immunol.* **7**, eabk2541 (2022).
36. A. R. Ellison, D. Wilcockson, J. Cable, Circadian dynamics of the teleost skin immune-microbiome interface. *Microbiome* **9**, 222 (2021).
37. A. C. Holloway, P. K. Reddy, M. A. Sheridan, J. F. Leatherland, Diurnal rhythms of plasma growth hormone, somatostatin, thyroid hormones, cortisol and glucose concentrations in rainbow trout, *Oncorhynchus mykiss*, during progressive food deprivation. *Biol. Rhythm Res.* **25**, 415–432 (1994).
38. S. Polakof, R. M. Ceinos, B. Fernández-Durán, J. M. Míguez, J. L. Soengas, Daily changes in parameters of energy metabolism in brain of rainbow trout: Dependence on feeding. *Comp. Biochem. Physiol. A Mol. Integr. Physiol.* **146**, 265–273 (2007).
39. P. K. Reddy, J. F. Leatherland, Does the time of feeding affect the diurnal rhythms of plasma hormone and glucose concentration and hepatic glycogen content of rainbow trout? *Fish Physiol. Biochem.* **13**, 133–140 (1994).
40. Y. Yang, M. Nguyen, V. Khetrapal, N. D. Sonnert, A. L. Martin, H. Chen, M. A. Kriegel, N. W. Palm, Within-host evolution of a gut pathobiont facilitates liver translocation. *Nature* **607**, 563–570 (2022).
41. J. W. Bledsoe, B. C. Peterson, K. S. Swanson, B. C. Small, Ontogenetic characterization of the intestinal microbiota of channel catfish through 16*S* rRNA gene sequencing reveals insights on temporal shifts and the influence of environmental microbes. *PLOS ONE* **11**, e0166379 (2016).
42. H. Sugita, T. Nakamura, Y. Deguchi, Identification of *Plesiomonas shigelloides* isolated from freshwater fish with the microplate hybridization method. *J. Food Prot.* **56**, 949–953 (1993).
43. V. Skrodenytė-Arbačiauskienė, A. Sruoga, D. Butkauskas, K. Skrupskelis, Phylogenetic analysis of intestinal bacteria of freshwater salmon *Salmo salar* and sea trout *Salmo trutta trutta* and diet. *Fish. Sci.* **74**, 1307–1314 (2008).
44. A. M. Larsen, H. H. Mohammed, C. R. Arias, Characterization of the gut microbiota of three commercially valuable warmwater fish species. *J. Appl. Microbiol.* **116**, 1396–1404 (2014).
45. A. Al-Hisnawi, E. Ringø, S. J. Davies, P. Waines, G. Bradley, D. L. Merrifield, First report on the autochthonous gut microbiota of brown trout (*Salmo trutta* Linnaeus). *Aquacult. Res.* **46**, 2962–2971 (2015).
46. S. Wu, T. Gao, Y. Zheng, W. Wang, Y. Cheng, G. Wang, Microbial diversity of intestinal contents and mucus in yellow catfish (*Pelteobagrus fulvidraco*). *Aquaculture* **303**, 1–7 (2010).
47. R. McDonald, H. J. Schreier, J. E. M. Watts, Phylogenetic analysis of microbial communities in different regions of the gastrointestinal tract in *Panaque nigrolineatus*, a wood-eating fish. *PLOS ONE* **7**, e48018 (2012).

48. M. Duman, E. García Valdés, H. Ay, S. Altun, I. B. Saticioglu, Description of a Novel Fish Pathogen, *Plesiomonas shigelloides subsp. oncorhynchi*, Isolated from Rainbow trout (*Oncorhynchus mykiss*): First genome analysis and comparative genomics. *Fishes* **8**, 179 (2023).
49. H. Chen, Y. Zhao, K. Chen, Y. Wei, H. Luo, Y. Li, F. Liu, Z. Zhu, W. Hu, D. Luo, Isolation, identification, and investigation of pathogenic bacteria from common carp (*Cyprinus carpio*) naturally infected with *Plesiomonas shigelloides*. *Front. Immunol.* **13**, 872896 (2022).
50. R. G. Nisha, V. Rajathi, R. Manikandan, N. M. Prabhu, Isolation of *Plesiomonas shigelloides* from infected cichlid fishes using 16*S* rRNA characterization and its control with probiotic *Pseudomonas* sp. *Acta Sci. Vet.* **42**, 1–7 (2014).
51. Z. Yin, S. Zhang, Y. Wei, M. Wang, S. Ma, S. Yang, J. Wang, C. Yuan, L. Jiang, Y. Du, Horizontal gene transfer clarifies taxonomic confusion and promotes the genetic diversity and pathogenicity of *Plesiomonas shigelloides*. *mSystems* **5**, e00448-20 (2020).
52. A. Nakamura, S. Kurihara, D. Takahashi, W. Ohashi, Y. Nakamura, S. Kimura, M. Onuki, A. Kume, Y. Sasazawa, Y. Furusawa, Symbiotic polyamine metabolism regulates epithelial proliferation and macrophage differentiation in the colon. *Nat. Commun.* **12**, 2105 (2021).
53. A. J. Michael, Polyamines in eukaryotes, bacteria, and archaea. *J. Biol. Chem.* **291**, 14896–14903 (2016).
54. S. Krysenko, W. Wohlleben, Polyamine and ethanolamine metabolism in bacteria as an important component of nitrogen assimilation for survival and pathogenicity. *Med. Sci.* **10**, 40 (2022).
55. K. Hamana, T. Akiba, F. Uchino, S. Matsuzaki, Distribution of spermine in bacilli and lactic acid bacteria. *Can. J. Microbiol.* **35**, 450–455 (1989).
56. K. Hamana, T. Tanaka, R. Hosoya, M. Niitsu, T. Itoh, Cellular polyamines of the acidophilic, thermophilic and thermoacidophilic archaebacteria, Acidilobus, Ferroplasma, Pyrobaculum, Pyrococcus, Staphylothermus, Thermococcus, Thermodiscus and Vulcanisaeta. *J. Gen. Appl. Microbiol.* **49**, 287–293 (2003).
57. D. Hyatt, G.-L. Chen, P. F. LoCascio, M. L. Land, F. W. Larimer, L. J. Hauser, Prodigal: Prokaryotic gene recognition and translation initiation site identification. *BMC Bioinformatics* **11**, 119 (2010).
58. S. Schroeder, S. J. Hofer, A. Zimmermann, R. Pechlaner, C. Dammbrueck, T. Pendl, G. M. Marcello, V. Pogatschnigg, M. Bergmann, M. Muller, Dietary spermidine improves cognitive function. *Cell Rep.* **35**, 108985 (2021).
59. C. Schwarz, G. S. Benson, N. Horn, K. Wurdack, U. Grittner, R. Schilling, S. Märschenz, T. Köbe, S. J. Hofer, C. Magnes, Effects of spermidine supplementation on cognition and biomarkers in older adults with subjective cognitive decline: A randomized clinical trial. *JAMA Netw. Open* **5**, e2213875 (2022).
60. Y. Yang, S. Chen, Y. Zhang, X. Lin, Y. Song, Z. Xue, H. Qian, S. Wang, G. Wan, X. Zheng, Induction of autophagy by spermidine is neuroprotective via inhibition of caspase 3-mediated Beclin 1 cleavage. *Cell Death Dis.* **8**, e2738 (2017).
61. L. A. Sandusky-Beltran, A. Kovalenko, C. Ma, J. I. T. Calahatian, D. S. Placides, M. D. Watler, J. B. Hunt, A. L. Darling, J. D. Baker, L. J. Blair, Spermidine/spermine-N1-acetyltransferase ablation impacts tauopathy-induced polyamine stress response. *Alzheimer's Res. Ther.* **11**, 58 (2019).
62. L. Glantz, J. L. Nates, V. Trembovler, R. Bass, E. Shohami, Polyamines induce blood-brain barrier disruption and edema formation in the rat. *J. Basic Clin. Physiol. Pharmacol.* **7**, 1–10 (1996).
63. D. T. Camak, M. J. Osborne, T. F. Turner, Population genomics and conservation of Gila Trout (*Oncorhynchus gilae*). *Conserv. Genet.* **22**, 729–743 (2021).
64. M. B. Peters, T. F. Turner, Genetic variation of the major histocompatibility complex (MHC class II β gene) in the threatened Gila trout, *Oncorhynchus gilae gilae*. *Conserv. Genet.* **9**, 257–270 (2008).
65. J. P. Wares, D. Alò, T. F. Turner, A genetic perspective on management and recovery of federally endangered trout (*Oncorhynchus gilae*) in the American Southwest. *Can. J. Fish. Aquat. Sci.* **61**, 1890–1899 (2004).
66. B. E. Riddell, R. D. Brodeur, A. V. Bugaev, P. Moran, J. M. Murphy, J. A. Orsi, M. Trudel, L. A. Weitkamp, B. K. Wells, A. C. Wertheimer, Ocean ecology of Chinook salmon, in *Ocean Ecology of Pacific Salmon and Trout* (American Fisheries Society, 2018), pp. 555–696.
67. R. K. Schroeder, L. D. Whitman, B. Cannon, P. Olmsted, Juvenile life-history diversity and population stability of spring Chinook salmon in the Willamette River basin, Oregon. *Can. J. Fish. Aquat. Sci.* **73**, 921–934 (2016).
68. C. E. Couch, M. E. Colvin, R. L. Chitwood, J. T. Peterson, C. B. Schreck, Scope of the cortisol stress response in Chinook salmon during maturation. *Fish. Res.* **254**, 106416 (2022).
69. S. C. Corbett, M. L. Moser, A. H. Dittman, Experimental evaluation of adult spring Chinook salmon radio-tagged during the late stages of spawning migration. *N. Am. J. Fish. Manag.* **32**, 853–858 (2012).
70. B. P. Dolan, K. M. Fisher, M. E. Colvin, S. E. Benda, J. T. Peterson, M. L. Kent, C. B. Schreck, Innate and adaptive immune responses in migrating spring-run adult chinook salmon, Oncorhynchus tshawytscha. *Fish Shellfish Immunol.* **48**, 136–144 (2016).
71. A. G. Maule, R. Schrock, C. Slater, M. S. Fitzpatrick, C. B. Schreck, Immune and endocrine responses of adult chinook salmon during freshwater immigration and sexual maturation. *Fish Shellfish Immunol.* **6**, 221–233 (1996).
72. T. A. Maldonado, *Distribution of Neurodegeneration, Amyloid Precursor Protein, β-Amyloid Peptide and Neuroprotection in the Brain of Migrating and Senescent Kokanee Salmon* (Univ. of Colorado Boulder, 2000).
73. M. S. Llewellyn, P. McGinnity, M. Dionne, J. Letourneau, F. Thonier, G. R. Carvalho, S. Creer, N. Derome, The biogeography of the atlantic salmon (*Salmo salar*) gut microbiome. *ISME J.* **10**, 1280–1284 (2016).
74. R. Mann, C. Caudill, M. Keefer, A. Roumasset, C. Schreck, M. Kent, "Migration behavior and spawning success of spring Chinook salmon in Fall Creek and the North Fork Middle Fork Willamette River: Relationships among fate, fish condition, and environmental factors 2010" (Technical report 2015-2).
75. S. Nervino, T. Polley, J. T. Peterson, C. B. Schreck, M. L. Kent, J. D. Alexander, Intestinal lesions and parasites associated with senescence and prespawn mortality in Chinook Salmon (*Oncorhynchus tshawytscha*). *J. Fish Dis.* **7**, e13876 (2024).
76. A. Varatharaj, I. Galea, The blood-brain barrier in systemic inflammation. *Brain Behav. Immun.* **60**, 1–12 (2017).
77. E. Elwood, Z. Lim, H. Naveed, I. Galea, The effect of systemic inflammation on human brain barrier function. *Brain Behav. Immun.* **62**, 35–40 (2017).
78. Y. Sun, Y. Koyama, S. Shimada, Inflammation from peripheral organs to the brain: How does systemic inflammation cause neuroinflammation? *Front. Aging Neurosci.* **14**, 903455 (2022).
79. C. Lobsinger, "Energy expenditure during breeding competition between feral Chinook salmon (*Oncorphynchus tshawytscha*) and native Atlantic salmon (*Salmo salar*)," thesis, University of British Columbia (2004).
80. T. A. Maldonado, R. E. Jones, D. O. Norris, Distribution of β-amyloid and amyloid precursor protein in the brain of spawning (senescent) salmon: A natural, brain-aging model. *Brain Res.* **858**, 237–251 (2000).
81. I. Vojtechova, T. Machacek, Z. Kristofikova, A. Stuchlik, T. Petrasek, Infectious origin of Alzheimer's disease: Amyloid beta as a component of brain antimicrobial immunity. *PLOS Pathog.* **18**, e1010929 (2022).
82. M. L. Gosztyla, H. M. Brothers, S. R. Robinson, Alzheimer's amyloid-β is an antimicrobial peptide: A review of the evidence. *J. Alzheimers Dis.* **62**, 1495–1506 (2018).
83. D. K. V. Kumar, S. H. Choi, K. J. Washicosky, W. A. Eimer, S. Tucker, J. Ghofrani, A. Lefkowitz, G. McColl, L. E. Goldstein, R. E. Tanzi, R. D. Moir, Amyloid-β peptide protects against microbial infection in mouse and worm models of Alzheimer's disease. *Sci. Transl. Med.* **8**, 340ra72 (2016).
84. T. A. Maldonado, R. E. Jones, D. O. Norris, Timing of neurodegeneration and beta-amyloid (Aβ) peptide deposition in the brain of aging kokanee salmon. *J. Neurobiol.* **53**, 21–35 (2002).
85. T. A. Maldonado, R. E. Jones, D. O. Norris, Intraneuronal amyloid precursor protein (APP) and appearance of extracellular β-amyloid peptide (Aβ) in the brain of aging kokanee salmon. *J. Neurobiol.* **53**, 11–20 (2002).
86. T. C. Fung, N. J. Bessman, M. R. Hepworth, N. Kumar, N. Shibata, D. Kobuley, K. Wang, C. G. K. Ziegler, J. Goc, T. Shima, Y. Umesaki, R. B. Sartor, K. V. Sullivan, T. D. Lawley, J. Kunisawa, H. Kiyono, G. F. Sonnenberg, Lymphoid-tissue-resident commensal bacteria promote members of the IL-10 cytokine family to establish mutualism. *Immunity* **44**, 634–646 (2016).
87. T. Obata, Y. Goto, N. Shibata, S. Sato, J. Kunisawa, H. Kiyono, Indigenous opportunistic bacteria inhabit mammalian gut-associated lymphoid tissues for mucosal antibody-mediated symbiosis. *Biol. Sci.* **107**, 7419–7424 (2010).
88. B. Novoa, T. V. Bowman, L. Zon, A. Figueras, LPS response and tolerance in the zebrafish (*Danio rerio*). *Fish Shellfish Immunol.* **26**, 326–331 (2009).
89. E. E. Adade, R. J. Stevick, D. Pérez-Pascual, J.-M. Ghigo, A. M. Valm, Gnotobiotic zebrafish microbiota display inter-individual variability affecting host physiology. bioRxiv 2023.02.01.526612 (2023). https://doi.org/10.1101/2023.02.01.526612.
90. M. Zhang, C. Shan, F. Tan, S. M. Limbu, L. Chen, Z.-Y. Du, Gnotobiotic models: Powerful tools for deeply understanding intestinal microbiota-host interactions in aquaculture. *Aquaculture* **517**, 734800 (2020).
91. E. Melancon, S. G. D. L. T. Canny, S. Sichel, M. Kelly, T. Wiles, J. Rawls, J. Eisen, K. Guillemin, Best practices for germ-free derivation and gnotobiotic zebrafish husbandry. *Methods Cell Biol.* **138**, 61–100 (2017).
92. D. Pérez-Pascual, S. Vendrell-Fernández, B. Audrain, J. Bernal-Bayard, R. Patiño-Navarrete, V. Petit, D. Rigaudeau, J.-M. Ghigo, Gnotobiotic rainbow trout (*Oncorhynchus mykiss*) model reveals endogenous bacteria that protect against *Flavobacterium columnare* infection. *PLOS Pathog.* **17**, e1009302 (2021).
93. S. G. de la Torre Canny, C. T. Nordgård, A. J. H. Mathisen, E. D. Lorentsen, O. Vadstein, I. Bakke, A novel gnotobiotic experimental system for Atlantic salmon (*Salmo salar* L.) reveals a microbial influence on mucosal barrier function and adipose tissue accumulation during the yolk sac stage. *Front. Cell. Infect. Microbiol.* **12**, 1068302 (2023).

94. D. Kim, C. E. Hofstaedter, C. Zhao, L. Mattei, C. Tanes, E. Clarke, A. Lauder, S. Sherrill-Mix, C. Chehoud, J. Kelsen, Optimizing methods and dodging pitfalls in microbiome research. *Microbiome* **5**, 52 (2017).
95. K. Noh, X. Liu, C. Wei, Optimizing transcardial perfusion of small molecules and biologics for brain penetration and biodistribution studies in rodents. *Biopharm. Drug Dispos.* **44**, 71–83 (2023).
96. P. Perdiguero, A. Martín-Martín, O. Benedicenti, P. Díaz-Rosales, E. Morel, E. Muñoz-Atienza, M. García-Flores, R. Simón, I. Soleto, A. Cerutti, Teleost IgD^+ IgM^- B cells mount clonally expanded and mildly mutated intestinal IgD responses in the absence of lymphoid follicles. *Cell Rep.* **29**, 4223–4235.e5 (2019).
97. L. de Nies, S. B. Busi, M. Tsenkova, R. Halder, E. Letellier, P. Wilmes, Evolution of the murine gut resistome following broad-spectrum antibiotic treatment. *Nat. Commun.* **13**, 2296 (2022).
98. C. M. Phelps, J. H. Shapira, C. R. Laughlin, M. Meisel, Detection of viable commensal bacteria in murine melanoma tumors by culturomics. *STAR Protocols* **4**, 102492 (2023).
99. K. R. Mitchell, C. D. Takacs-Vesbach, A comparison of methods for total community DNA preservation and extraction from various thermal environments. *J. Ind. Microbiol. Biotechnol.* **35**, 1139–1147 (2008).
100. E. Bolyen, J. R. Rideout, M. R. Dillon, N. A. Bokulich, C. C. Abnet, G. A. Al-Ghalith, H. Alexander, E. J. Alm, M. Arumugam, F. Asnicar, Y. Bai, J. E. Bisanz, K. Bittinger, A. Brejnrod, C. J. Brislawn, C. T. Brown, B. J. Callahan, A. M. Caraballo-Rodríguez, J. Chase, E. K. Cope, R. D. Silva, C. Diener, P. C. Dorrestein, G. M. Douglas, D. M. Durall, C. Duvallet, C. F. Edwardson, M. Ernst, M. Estaki, J. Fouquier, J. M. Gauglitz, S. M. Gibbons, D. L. Gibson, A. Gonzalez, K. Gorlick, J. Guo, B. Hillmann, S. Holmes, H. Holste, C. Huttenhower, G. A. Huttley, S. Janssen, A. K. Jarmusch, L. Jiang, B. D. Kaehler, K. B. Kang, C. R. Keefe, P. Keim, S. T. Kelley, D. Knights, I. Koester, T. Kosciolek, J. Kreps, M. G. I. Langille, J. Lee, R. Ley, Y.-X. Liu, E. Loftfield, C. Lozupone, M. Maher, C. Marotz, B. D. Martin, D. M. Donald, L. J. McIver, A. V. Melnik, J. L. Metcalf, S. C. Morgan, J. T. Morton, A. T. Naimey, J. A. Navas-Molina, L. F. Nothias, S. B. Orchanian, T. Pearson, S. L. Peoples, D. Petras, M. L. Preuss, E. Pruesse, L. B. Rasmussen, A. Rivers, M. S. Robeson II, P. Rosenthal, N. Segata, M. Shaffer, A. Shiffer, R. Sinha, S. J. Song, J. R. Spear, A. D. Swafford, L. R. Thompson, P. J. Torres, P. Trinh, A. Tripathi, P. J. Turnbaugh, S. Ul-Hasan, J. J. J. van der Hooft, F. Vargas, Y. Vázquez-Baeza, E. Vogtmann, M. von Hippel, W. Walters, Y. Wan, M. Wang, J. Warren, K. C. Weber, C. H. D. Williams, A. D. Willis, Z. Z. Xu, J. R. Zaneveld, Y. Zhang, Q. Zhu, R. Knight, J. G. Caporaso, Reproducible, interactive, scalable and extensible microbiome data science using QIIME 2. *Nat. Biotechnol.* **37**, 852–857 (2019).
101. B. J. Callahan, P. J. McMurdie, M. J. Rosen, A. W. Han, A. J. A. Johnson, S. P. Holmes, DADA2: High-resolution sample inference from Illumina amplicon data. *Nat. Methods* **13**, 581–583 (2016).
102. C. Quast, E. Pruesse, P. Yilmaz, J. Gerken, T. Schweer, P. Yarza, J. Peplies, F. O. Glöckner, The SILVA ribosomal RNA gene database project: Improved data processing and web-based tools. *Nucleic Acids Res.* **41**, D590–D596 (2012).
103. J. E. Bisanz, *qiime2R: Importing QIIME2 Artifacts and Associated Data Into R Sessions* (2018); R Package version 0.99.
104. D. Knights, J. Kuczynski, E. S. Charlson, J. Zaneveld, M. C. Mozer, R. G. Collman, F. D. Bushman, R. Knight, S. T. Kelley, Bayesian community-wide culture-independent microbial source tracking. *Nat. Methods* **8**, 761–763 (2011).
105. Y. Liu, R. A. L. Elworth, M. D. Jochum, K. M. Aagaard, T. J. Treangen, De novo identification of microbial contaminants in low microbial biomass microbiomes with Squeegee. *Nat. Commun.* **13**, 6799 (2022).
106. O. Zemb, C. S. Achard, J. Hamelin, M. De Almeida, B. Gabinaud, L. Cauquil, L. M. G. Verschuren, J. Godon, Absolute quantitation of microbes using 16*S* rRNA gene metabarcoding: A rapid normalization of relative abundances by quantitative PCR targeting a 16*S* rRNA gene spike-in standard. *Microbiology Open* **9**, e977 (2020).
107. A. Leger, T. Leonardi, pycoQC, interactive quality control for Oxford nanopore sequencing. *J. Open Source Softw.* **4**, 1236 (2019).
108. K. Shafin, T. Pesout, R. Lorig-Roach, M. Haukness, H. E. Olsen, C. Bosworth, J. Armstrong, K. Tigyi, N. Maurer, S. Koren, F. J. Sedlazeck, T. Marschall, S. Mayes, V. Costa, J. M. Zook, K. J. Liu, D. Kilburn, M. Sorensen, K. M. Munson, M. R. Vollger, J. Monlong, E. Garrison, E. E. Eichler, S. Salama, D. Haussler, R. E. Green, M. Akeson, A. Phillippy, K. H. Miga, P. Carnevali, M. Jain, B. Paten, Nanopore sequencing and the Shasta toolkit enable efficient de novo assembly of eleven human genomes. *Nat. Biotechnol.* **38**, 1044–1053 (2020).
109. T. Seemann, Prokka: Rapid prokaryotic genome annotation. *Bioinformatics* **30**, 2068–2069 (2014).
110. S. Deorowicz, A. Debudaj-Grabysz, A. Gudyś, FAMSA: Fast and accurate multiple sequence alignment of huge protein families. *Sci. Rep.* **6**, 33964 (2016).
111. A. M. Eren, Ö. C. Esen, C. Quince, J. H. Vineis, H. G. Morrison, M. L. Sogin, T. O. Delmont, Anvi'o: An advanced analysis and visualization platform for 'omics data. *PeerJ* **3**, e1319 (2015).
112. L.-T. Nguyen, H. A. Schmidt, A. Von Haeseler, B. Q. Minh, IQ-TREE: A fast and effective stochastic algorithm for estimating maximum-likelihood phylogenies. *Mol. Biol. Evol.* **32**, 268–274 (2015).
113. L. Jelsbak, L. E. Thomsen, I. Wallrodt, P. R. Jensen, J. E. Olsen, Polyamines are required for virulence in Salmonella enterica serovar Typhimurium. *PLOS ONE* **7**, e36149 (2012).

Acknowledgments: We thank D. Dinwiddie for sharing the Illumina sequencer used in this project and the University of New Mexico Center for Advanced Research Computer (CARC) for computational resources and data storage support. We thank M. Paffett at the University of New Mexico Cancer Research Facility for microscopy support. We thank J. O. Sunyer's laboratory for providing the labeled Plesiomonas strain. We thank New Mexico Fish and Wildlife for supplying the Gila trout specimens used in this study, L. Whitman and other personnel from the Oregon Department of Fisheries and Wildlife (ODFW) for Chinook salmon samples, and M. Kent for providing the Chinook salmon paraffin blocks. We thank M. Meisel, V. Martinson, and Y. Yang for helpful feedback on methods and data analysis for this manuscript. We thank Vaxxinova Norway and Marine RASlab for providing Atlantic salmon and H. Kvalvik at the Norwegian Veterinary Institute for help with sampling. **Funding:** This work was supported by the National Institutes of Health (grant NCI P30CA118100; UNM Comprehensive Cancer Center) and the Norwegian Department of Fisheries through the Norwegian Veterinary Institute. **Author contributions:** Conceptualization: I.S. and A.M. Methodology: A.M., C.C., and I.S. Investigation: A.M., C.C., C.H., and I.S. Sample collection: A.M., C.C., T.L., J.T.H.C., S.P., and T.K. Visualization: A.M. and I.S. Bioinformatics analysis: A.M. Funding acquisition: I.S. Project administration: I.S. Supervision: I.S. Writing—original draft: A.M. and I.S. Writing—review and editing: A.M., I.S., C.C., C.H., T.L., J.T.H.C., S.P., and T.K. **Competing interests:** The authors declare that they have no competing interests. **Data and materials availability:** All data needed to evaluate the conclusions in the paper are present in the paper and/or the Supplementary Materials. All 16*S* ribosomal DNA amplicon sequencing data and bacterial whole-genome sequencing have been submitted to the National Center for Biotechnology Information (NCBI) Sequence Read Archive (SRA) under Bioproject accession numbers PRJNA1033688 and PRJNA1032609, respectively.

Submitted 12 January 2024
Accepted 12 August 2024
Published 18 September 2024
10.1126/sciadv.ado0277